Progress Report on the Performed Work During the 1st Year of the DOE Nuclear Engineering Education Research (NEER) Grant
Grant No. 03ID14497

A NEW METHODOLOGY FOR EARLY ANOMALY DETECTION OF BWR INSTABILITIES

Principal Investigator: Kostadin N. Ivanov
The Pennsylvania State University
230 Reber Building
University Park, PA 16802
Phone: (814) 865-0040
Fax: (814) 865-8499
Email: kni1@psu.edu

Submitted:

June 2004

Contents

1 Project Abstract

Project Title: A New Methodology for Early Anomaly Detection of BWR Instabilities

Participant: Kostadin Ivanov, The Pennsylvania State University, (814) 865-0040, kni1@psu.edu

The objective of the performed research is to develop an early anomaly detection methodology so as to enhance safety, availability, and operational flexibility of Boiling Water Reactor (BWR) nuclear power plants. The technical approach relies on suppression of potential power oscillations in BWRs by detecting small anomalies at an early stage and taking appropriate prognostic actions based on an anticipated operation schedule.

The research utilizes a model of coupled (two-phase) thermal-hydraulic and neutron flux dynamics, which is used as a generator of time series data for anomaly detection at an early stage. The model captures critical nonlinear features of coupled thermal-hydraulic and nuclear reactor dynamics and (slow time-scale) evolution of the anomalies as non-stationary parameters. The time series data derived from this nonlinear non-stationary model serves as the source of information for generating the symbolic dynamics for characterization of model parameter changes that quantitatively represent small anomalies. The major focus during the 1st year research activity was on developing algorithms of pattern recognition for power instability based on anomaly detection from time series data, which later can be used to formulate real-time decision and control algorithms for suppression of power oscillations for a variety of anticipated operating conditions.

The research being performed in the framework of this project is essential to make significant improvement in the capability of thermal instability analyses for enhancing safety, availability, and operational flexibility of currently operating and next generation BWRs.

2 Contact and Biographical Information

Kostadin N. Ivanov

Professor of Nuclear Engineering

Nuclear Engineering Program, Department of Mechanical and Nuclear Engineering
The Pennsylvania State University, 230 Reber Building, University Park, PA 16802
Phone: (814) 865-0040 Fax: (814) 865-8499

DEGREES:

P.E. (1982) – Nuclear Engineering, Moscow Institute of Power Engineering
Ph.D. (1990) – Reactor Physics, Institute of Nuclear Research and Nuclear Energy, Bulgarian Academy of Sciences

RELATED EXPERIENCE:

August 1999 – present - The Pennsylvania State University, Department of Mechanical and Nuclear Engineering, Nuclear Engineering Program, Associate Professor
August 1997–July 1999 – The Pennsylvania State University, Department of Mechanical and Nuclear Engineering, Nuclear Engineering Program, Assistant Professor
January 1996-July 1997 – The Pennsylvania State University, Department of Nuclear Engineering, Research Associate
June 1995-January 1996-Research Center Rossendorf Inc., Germany Institute for Safety Research, Department of Transient Analysis, Visiting Scientist
1993-1995 – The Pennsylvania State University, Department of Nuclear Engineering, Visiting Research Scholar
1987-1993 – Institute of Nuclear Research and Nuclear Energy, Sofia, Bulgaria, Department of Neutron and Reactor Physics, Senior Research Scientist
1991-1993 – Technical University of Sofia, Sofia, Bulgaria, Department of Nuclear Engineering, Assistant Professor
1985-1987 - Institute of Nuclear Research and Nuclear Energy, Sofia, Bulgaria, Department of Neutron and Reactor Physics, Research Scientist
1984-1985 – Kozloduy Nuclear Power Plants, Kozloduy, Bulgaria, Research Division, Physicist
1982-1984 – Kozloduy Nuclear Power Plants, Kozloduy, Bulgaria, Operation Division, Nuclear Engineer

EXPERTISE

Reactor physics; Development of methods and computer codes for multidimensional reactor core analysis; Nuclear fuel management and reloading optimisation techniques; Reactor kinetics and core dynamics; Cross-section generation and modelling algorithms; Coupling three-dimensional (3-D) kinetics models with thermal-hydraulic codes; Validation/verification of reactor core simulators, coupled code qualification and feedback testing;

TEACHING

Basic Reactor Physics Courses, Senior Reactor Design Course, Nuclear Reactor Statics and Fuel Management, and Reactor Kinetics and Dynamics.

PRINCIPAL PUBLICATIONS

1. J. Solis, M. Avramova, and K. Ivanov, "Temporal Adaptive Algorithm for TRAC-BF1/NEM/COBRA-TF Coupled Calculations in BWR Safety Analysis", Annals of Nuclear Energy, 29 (2002) 2127-2141.
2. J. Solis, J., H. Fu, K. Ivanov, Y. Matsui, A. Hotta, "Developing and Modeling of the Laguna Verde BWR CRDA Benchmark", Annals of Nuclear Energy, 29 (2002) 585-593.
3. J. Watson, and K. Ivanov, "Improved Cross-Section Modeling Methodology for Coupled Three-Dimensional Transient Calculations", Annals of Nuclear Energy 29 (2002) 937-966.
4. K. Ivanov et al, "Multidimensional TMI-1 Main Steam Line Break Analysis Methodology Using TRAC-PF1/NEM", Nuclear Technology, Vol. 133, No. 2, p. 169-186 (2001)
5. D. Ziabletsev and K. Ivanov, "Improved Verification Methodology for TRAC-PF1/NEM Using OECD/NEA Core Transient Benchmarks", Annals of Nuclear Energy 27/14 (2000), 1319-1331.
6. B. Taylor and K. Ivanov, "Statistical Methods Used for Code-to-Code Comparisons in the OECD/NRC PWR MSLB Benchmark" Annals of Nuclear Energy 27/17 (2000), 1589-1605.
7. H. Fu, J. Solis-Rodarte and K. Ivanov, "TRAC-BF1/NEM Modeling and Results of OECD/NEA BWR Core Transient Benchmarks", Annals of Nuclear Energy 27/12 (2000), 1051-1058.
8. J. Solis-Rodarte, K. Ivanov et al, "TRAC-BF1/NEM Stability methodology for BWR Core Wide and Regional Stability Analysis", Annals of Nuclear Energy 27/11 (2000), 985-994.
9. K. Ivanov et al, "PWR MSLB Benchmark. Volume 1: Final Specifications", NEA/NSC/DOC(99)8, April 1999, US NRC and OECD NEA.
10. K. Ivanov, U. Grundmann, S. Mittag, U. Rohde, "Comparative Study of a Boron Dilution Scenario in VVER Reactors", Annals of Nuclear Energy, 26 (1999) 1331-1335
11. K. Ivanov, R. Macian, A. Irani, A. Baratta, "Features and Performance of a Coupled Three-Dimensional Thermal Hydraulic/Kinetics PWR Analysis Code TRAC-PF1/NEM", Annals of Nuclear Energy, 26 (1999) 1407-1417
12. T. Beam, K. Ivanov, A. Baratta, H. Finnemann, "Nodal Kinetics Model Upgrade in the Penn State Coupled TRAC/NEM Codes", Annals of Nuclear Energy, 26 (1999) 1205-1219
13. R. Macian, K. Ivanov, and J. Mahaffy, "Numerical Diffusion and the Tracking of Solute Fields in system codes. Part III: Application to a Boron Dilution Transient Analysis in the AP600", Nuclear Engineering and Design, 179, p. 345 (1998).
14. T. Apostolov, G. Alekova, and K. Ivanov, "Comparative Analysis of WWER-1000 Benchmark Calculations and Improvements in Hexagonal-Z Diffusion Methodology", Annals of Nuclear Energy, Vol. 25, No. 1-3, p. 83 (1998).
15. B. Bandini, K. Ivanov, A. Baratta, and R. Steinke, "Verification of a Three-Dimensional Nodal Transient Neutronics Routine for the TRAC-PF1/MOD3 Thermal-Hydraulic System Analysis Code", Nuclear Technology, Vol. 123, p. 1 (1998).
16. M. Manolova, K. Ivanov, T. Apostolov, "A Hexagonal-Z Diffusion Theory Burnup Model for FBR Core Design Study", Kerntechnik, 60, p. 175 (1995).
17. K. Ivanov, M. Manolova, T. Apostolov – INRNE, Sofia, Bulgaria A. Seriogin, A. Chebeskov, V. Cherny-IPPE, Obninsk, Russia "Verification of HEXAB-3D Code on the BN-1600 Three-Dimensional Fast Power Reactor Model", VANT, Ser. "Nuclear Reactor Physics and Calculational Methods", 3, p. 82, (1994).
18. K. Ivanov, M. Manolova, T. Apostolov, "An Effective Solution Scheme of a Three-Dimensional Core Model in Hexagonal Geometry", Computer Physics Communications, 82, pp. 1-16 (1994).
19. K. Ivanov, M. Manolova, T. Apostolov, "Multi-Level Optimization of Improved Coarse-Mesh Steady-State Diffusion Calculations in Hexagonal-Z Geometry", "Journal of Bulgarian Academy of Sciences", Vol. 47, #7, p.31 (1994).
20. K. Ivanov, T. Apostolov, M. Manolova, "The HEXAB-3D Three-Dimensional Few-Group Improved Coarse-Mesh Diffusion Code in Hexagonal-Z Geometry", Nuclear Science and Engineering, Vol. 114, #2 p. 176 (1993).

3 DESCRIPTION OF PERFORMED WORK

3.1 Objectives

The objective of this research, which is supported by the US Department of Energy under the NEER program, is to develop an early anomaly detection methodology in order to enhance safety, availability, and operational flexibility of Boiling Water Reactor (BWR) nuclear power plants. The technical approach relies on suppression of potential power oscillations in BWRs by detecting small anomalies at an early stage and taking appropriate prognostic actions based on an anticipated operation schedule.

The model of coupled (two-phase) thermal-hydraulic and neutron flux dynamics, based on the US NRC coupled code TRACE/PARCS[1,2], is being used as a generator of time series data for anomaly detection at an early stage. The model captures critical nonlinear features of coupled thermal-hydraulic and nuclear reactor dynamics and (slow time-scale) evolution of the anomalies as non-stationary parameters. The time series data derived from this nonlinear non-stationary model serves as the source of information for generating the symbolic dynamics for characterization of model parameter changes that quantitatively represent small anomalies. This information is then used to develop algorithms of pattern recognition for power instability based on anomaly detection from time series data and to formulate real-time decision and control algorithms for suppression of power oscillations for a variety of anticipated operating conditions.

3.2 Development of Anomaly Detection Methodology

The performed work during the first year of the project, which is described in this paper, focused on the construction of proposed anomaly detection methodology[3]. The concept is based on the fact that nonlinear systems show bifurcation, which is a change in the qualitative behavior as the system parameters vary. Some of these parameters may change on their own accord and account for the anomaly, while certain parameters can be altered in a controlled fashion.

The non-linear, non-autonomous BWR system model considered in this research exhibits phenomena at two time scales. Anomalies occur at the slow time scale while the observation of the dynamical behavior, based on which inferences are made, takes place at the fast time scale. It is assumed that: (i) the system behavior is stationary at the fast time scale; and (ii) any observable non-stationary behavior is associated with parametric changes evolving at the slow time scale. The goal is to make inferences about evolving anomalies based on the asymptotic behavior derived from the computer simulation. However, only sufficient changes in the slowly varying parameter may lead to detectable difference in the asymptotic behavior. The need to detect such small changes in parameters and hence early detection of an anomaly motivates the utilized stimulus-response approach. In this approach, the model of a BWR system is perturbed with an appropriate known input excitation to observe the asymptotic behavior at the fast time scale. A set of suitable input excitation parameters or stimuli are employed and the separate response of the BWR system to each of these stimuli is determined. As a result of the combination of the input stimulus and perturbed parameter(s), it is possible to observe a detectable change in the nature of asymptotic behavior that would otherwise remain unperceivable over a long period of time.

The developed anomaly detection methodology is built upon the concepts of *Symbolic Dynamics*, *Finite State Automata*, and *Pattern Recognition* to qualitatively describe the dynamical behavior in terms of symbol sequences at the *fast-time* scale[4]. Appropriate phase space partitioning of the dynamical system yields an alphabet to obtain symbol sequences from time series data. To identify statistical patterns in these symbolic sequences, the tools of Computational Mechanics are used through construction of a

(probabilistic) finite-state machine from each symbol sequence. Transition probability matrices of the finite state machines, obtained from the symbol sequences, capture the pattern of the system behavior by information compression. A detectable change in the pattern represents a deviation of the nominal behavior from an anomalous one and suffices for anomaly detection. The state probability vectors derived from the respective connection (state transition) matrices under the nominal and an anomalous condition, yield a vector measure of the anomaly. This vector measure provides more information than a scalar measure such as the complexity measure.

In contrast to the e-machine that has an *a priori* unknown structure and yields optimal pattern discovery in the sense of mutual information, the state machine adopted here has an *a priori* known structure that can be freely chosen. Although this approach is suboptimal, it provides a common state machine structure where physical significance of each state is invariant under changes in the statistical patterns of symbol sequences. This feature allows unambiguous detection of possible anomalies from symbol sequences at different (slow-time) epochs. This fixed structure fixed-order Markov chain called the *D*-Markov machine is apparently computationally faster than the e-machine because of significantly fewer number of floating point arithmetic operations. These are the motivating factors for introducing the *D*-Markov machine. The machines described above recognize patterns in the behavior of a dynamical system that undergoes anomalous behavior. In order to quantify changes in the patterns that are representations of evolving anomalies, we induce an *anomaly measure* on these machines denoted by $\boldsymbol{M}$.

The anomaly detection methodology is separated into two parts:

i) Forward problem;
ii) Inverse problem.

The first year activity described here has been concentrated on the forward problem to build a firm foundation for further development of the methodology. The objective in the forward problem is to learn how the grammar underlying the system dynamics changes as the system parameters change. In other words, the forward problem is that of learning where the value of a parameter is associated with an anomaly measure. The following steps are identified to solve the forward problem:

1. Selection of appropriate Input Stimuli.

2. Signal-noise separation, time interval selection, and phase-space construction.

3. Choice of a phase space partitioning to generate Symbolic Dynamics.

4. State Machine construction using generated symbol sequence(s) and determining the connection matrix.

5. Selection of an appropriate metric for the anomaly measure *M*.

6. Formulation and calibration of a (possibly non-parametric) relation between the computed anomaly measure and known physical anomaly under which the time series data were collected at different (slow-time) epochs.

3.2.1 Symbolic Dynamics and Encoding

This section introduces the concept of *Symbolic Dynamics* and its usage for encoding nonlinear system dynamics from observed time series data. Let a continuously varying physical process be modeled as a finite-dimensional system in the setting of an initial value problem as:

$$\frac{dx(t)}{dt} = f(x(t), q); \; x(0) = x_0 \tag{3.1}$$

where $t \in [0, \infty)$ is the time; $x \in \Re^n$ is the state vector in the *phase space*; and $q \in \Re^m$ is the (possibly slowly) varying parameter vector. The sole usage of the model in the Equation 3.1 may not always be feasible due to unknown parametric and non-parametric uncertainties and noise. A convenient way of learning the dynamical behavior is to rely on the additional information provided by (sensor-based) time series data.

A tool for behavior description of nonlinear dynamical systems is based on the concept of Formal Languages for transitions from smooth dynamics to a discrete symbolic description. The phase space of the dynamical system in the above equation is partitioned into a finite number of cells, so as to obtain a coordinate grid of the space. For simplicity, a compact (i.e., closed and bounded) region $\Omega \subseteq R^n$ within which the motion is circumscribed is identified with the phase space itself. The encoding of Ω is accomplished by introducing a $B \equiv \{B_0, \cdots, B_{b-1}\}$ consisting of n_b mutually exclusive (i.e., $B_j \bigcap B_k = \varnothing$, $\forall j \neq k$) and exhaustive (i.e., $\bigcup_{j=0}^{n_b - 1} \boldsymbol{B}_j = \Omega$) cells. The dynamical system describes an orbit $O \equiv \{x_0, x_1 \cdots, x_n \cdots\}$ which passes through or touches the cells of the partition B. Let us denote the index of domain visited at the time instant *i* as the symbol $\boldsymbol{s_i} \in \mathrm{A}$, where the set A of n_b distinct symbols that labels the partition elements is called the *symbol alphabet*. (Note: A symbol alphabet A is called a generating partition of the phase space Ω if a legal, i.e., physically admissible, symbol sequence uniquely determines a specific initial condition x_0, implying that the mapping from the phase space to the symbol space is bijective) Each initial state x_0 in Ω generates a sequence of symbols defined by a mapping from the phase space to the symbol space as:

$$\boldsymbol{x}_0 \mapsto \boldsymbol{s_i}\, \boldsymbol{s_j} \cdots \boldsymbol{s_n} \cdots \tag{3.2}$$

The mapping in the Equation (3.2) is called Symbolic Dynamics as it attributes a legal symbol sequence to the system dynamics starting from an initial state. Although the theory of symbolic dynamics is well developed for one-dimensional mappings, very few results are known for two and higher dimensional systems. Recently, a technique for obtaining generating partition directly from the time series has been proposed by Kennel and Buhl. Figure 3.1 elucidates partitioning of a finite region of a phase space and a mapping from the partitioned space into the symbol alphabet, which becomes a representation of the system dynamics defined by the trajectories. It also shows the conversion of the symbol sequence into a finite state machine as explained in later sections.

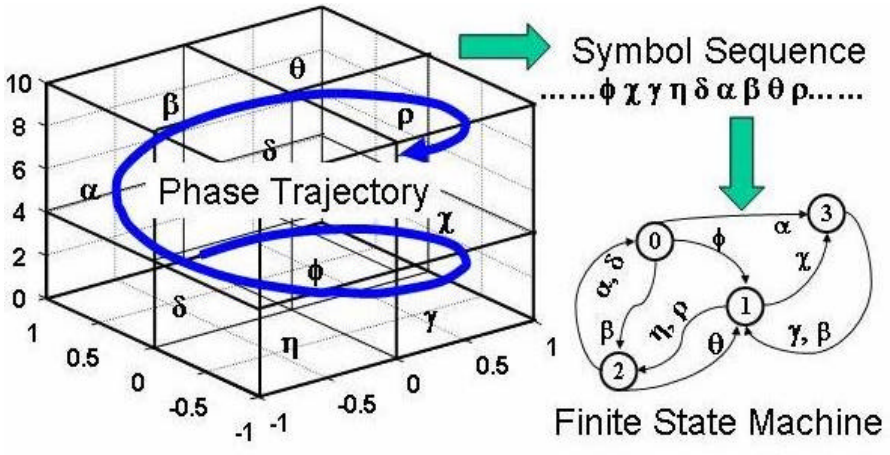

Figure 3.1 Phase Space Partitioning

Finding a partitioning is a difficult task especially if the time series data is noise-contaminated. Several methods of phase-space partitioning have been suggested in literature. Apparently, there exist no well-established procedure for phase-space partitioning and this is a subject of active research.

We have used two approaches to find the partitioning needed to construct the symbol sequence. The first approach is the symbolic false nearest neighbors (SFNN) approach by Kennel and Buhl. The objective of this approach is to find a "generating" partition, where symbolic orbits uniquely identify one continuous space orbit, and thus the symbolic dynamics is fully equivalent to the continuous space dynamics. The method optimizes an essential property of a generating partition: avoiding topological degeneracies. The criterion is that short sequences of consecutive symbols ought to localize the corresponding state space point as well as possible. The central idea is to form a particular geometrical embedding of the symbolic sequence under the candidate partition and evaluate, and minimize, a statistics, which quantifies the apparent errors in localizing state space points. In a good partition, nearby points in the embedding remain close when mapped back into the state space. By contrast bad partitions induce topological degeneracies where symbolic words map back to globally distinct regions of state space. The *nearest neighbor*, in Euclidean distance, to each point in the embedding is found. Knowing symbolic neighbors, we find distances of those same points back in state space. Better partitions give a smaller proportion of *symbolic false nearest neighbors*. For concrete numerical calculations, the partitions are parameterized with a relatively small number of free parameters by defining the partitions with respect to a set of radial-basis "influence" functions. The statistics for symbolic false nearest neighbors is minimized over the free parameters using "differential evolution", a genetic algorithm suitable for continuous parameter spaces.

The second approach used, we will hereby call the wavelet space (WS) method is a new approach that we have introduced and that uses wavelet transform to convert the time series data to time-frequency data for generating the symbol sequence. The graphs of wavelet coefficients versus scale at selected time shifts are stacked starting with the smallest value of scale and ending with its largest value and then back from the largest value to the smallest value of the scale at the next instant of time shift. The resulting *scale series* data in the wavelet space is analogous to the time series data in the phase space. Then, the wavelet space is partitioned into segments of coefficients on the ordinate separated by horizontal lines. The

number of segments in a partition is equal to the size of the alphabet and each partition is associated with a symbol in the alphabet.

Having defined a partition, the time series or scale series data is converted to a symbol sequence that, in turn, is used for construction of a finite state machine using the tools of Computational Mechanics. Two alternative techniques of finite-state machine construction are: (i) the e-machine construction; and (ii) a new technique based on D^{th} order Markov chains, called the *D*-Markov machine, for identifying patterns based on time series analysis of the observed data. Both techniques rely on information-theoretic principles and are based on Computational Mechanics. The anomaly detection methodology implemented in this research utilizes the *D*-Markov machine for finite-state machine construction.

3.2.2 The Suboptimal *D*-Markov Machine

This section describes the implemented technique for representing the pattern in a symbolic process, which is motivated from the perspective of anomaly detection. The core assumption here is that the symbolic process can be represented to a desired level of accuracy as a D^{th} order Markov chain, by appropriately choosing $\boldsymbol{D \in N}$. A stochastic symbolic stationary process $\boldsymbol{S \equiv .., s_{-2}s_{-1}s_0s_1s_2\cdots}$, is called D^{th} order Markov Process if the probability of the next symbol depends only on the previous *D* symbols, i.e. the following condition holds:

$$\boldsymbol{P(s_i \mid s_{i-1}s_{i-2}\ldots) = P(s_i \mid s_{i-1}..s_{i-D})} \tag{3.3}$$

For a given $\boldsymbol{D \in N}$ and neglecting the transient states, we define the following *effective* states of the symbolic process:

$$\boldsymbol{Q = \{s^D : s^D \in A^D\}} \tag{3.4}$$

The random vector for the above set of states is denoted by $\boldsymbol{Q}$ and the *i*th state as q_i. Given an initial state and the next symbol from the original process, only certain successor states are possible. This is represented as the allowed transitions between the states and the probabilities of these transitions as:

$$\boldsymbol{T_{ij}^{(s)} = P(\overrightarrow{S}^1 = s, Q' = q_j \mid Q = q_i)} \tag{3.5}$$

for all $\boldsymbol{q_i, q_j \in Q}$. Note that $\boldsymbol{T_{ij}^{(s)} = 0}$ for $\boldsymbol{q_i = s_1s_2...s_D}$ and s $\boldsymbol{q_j = s'_1s'_2...s'_D}$ such that $\boldsymbol{s_2s_3...s_D \neq s'_1...s'_D}$. Thus, the stochastic matrix *T* is a branded matrix with at most $\boldsymbol{|A^{D+1}|}$ nonzero entries.

The construction of a *D*-Markov machine is fairly straightforward. On a given symbol sequence, a window of length *D+1* is slided by keeping a count of the frequency of occurrence of sequences $\boldsymbol{s_1..s_Ds_{D+1}}$ and $\boldsymbol{s_1...s_D}$ which are respectively denoted by $\boldsymbol{N(s_1...s_Ds_{D+1})}$ and $\boldsymbol{N(s_1...s_D)}$. Note that if $\boldsymbol{N(s_1...s_D) = 0}$ then the state $\boldsymbol{q = s_1...s_D \in Q}$ does not exist. The transitions probabilities are then obtained by these frequency counts as follows, (for $\boldsymbol{N(s_1...s_D) \neq 0}$):

$$T_{ij}^{(s)} = \frac{P(s_1 \ldots s_D s)}{P(s_1 \ldots s_D)} = \frac{N(s_1 \ldots s_D s)}{N(s_1 \ldots s_D)} \tag{3.6}$$

where, $q_i = s_1 \ldots s_D$ and $q_j = s_2 \ldots s_D s$.

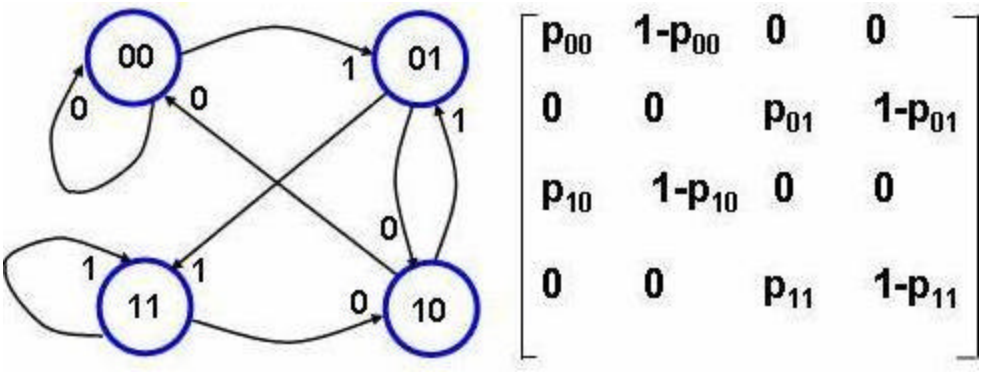

Figure 3.2 State Machine with *D*=2, and |*A*|=2

As an example, Figure 3.2 shows construction of the finite state machine and the associated state transition matrix for a *D*-Markov process, where the alphabet size $|A| = 2$ and the states are chosen as words of length *D*=2 from the symbol sequence. Therefore, the total number of states is $|A|^D = 4$, which is the number of permutations of the alphabet symbols within a word of length *D*. The states are joined by edges labeled by a symbol in the alphabet. The state machine moves from one state to another upon occurrence of an event as a new symbol in the symbol sequence is received. The machine language is complete in the sense that there are different outgoing edges marked by different symbols; however, it is possible that the some of these arcs may have zero probability.

In general, the effects of an anomaly are reflected in the respective state transition matrices. Thus, the structure of the finite state machine is fixed for a given alphabet size and window length *D*. Furthermore, the number of edges is also finite because of the finite alphabet size. The elements of the state transition matrix (that is a stochastic matrix) are identified from the symbol sequence.

3.2.3 Anomaly Measure and Detection

The machines described above recognize patterns in the behavior of a dynamical system that undergoes anomalous behavior. In order to quantify changes in the patterns that are representations of evolving anomalies, we induce an *anomaly measure* on these machines denoted by ***M***. The anomaly measure ***M*** can be constructed based on the following information-theoretic quantities: entropy rate, excess entropy, and complexity measure of a symbol string ***S***.

- The entropy rate $h_m(S)$ quantifies the intrinsic randomness in the observed dynamical process.
- The excess entropy **E**(***S***) quantifies the memory in the observed process.
- The statistical complexity $C_m(S)$ of the state machine captures the average memory requirements for modeling the complex behavior of a process.

Given two symbol strings ***S*** and S_0 it is possible to obtain a measure of anomaly by adopting any one of the following three alternatives:

$$\boldsymbol{M}(\boldsymbol{S},\boldsymbol{S}_0)=\begin{cases}|\,\boldsymbol{h}_m(\boldsymbol{S})-\boldsymbol{h}_m(\boldsymbol{S}_0)\,|, or\\ |\,\mathrm{E}(\boldsymbol{S})-\mathrm{E}(\boldsymbol{S}_0)\,|, or\\ |\,\boldsymbol{C}_m(\boldsymbol{S})-\boldsymbol{C}_m(\boldsymbol{S}_0)\,|\end{cases} \tag{3.7}$$

Note that each of the anomaly measures, defined above, is a *pseudo metric*. For example, let us consider two periodic processes with unequal periods, represented by $\boldsymbol{S}$ and $\boldsymbol{S_0}$. For both processes $\boldsymbol{h}_m = 0$, so that $\boldsymbol{M}(\boldsymbol{S},\boldsymbol{S}_0)=0$ for the first of the above three options, even if $\boldsymbol{S}\neq\boldsymbol{S}_0$.

The above measures are obtained through scalar-valued functions defined on a state machine and do not exploit the rich algebraic structure represented in the state machine. For example, the connection matrix *T* associated with the e-machine can be treated as a vector representation of any possible anomalies in the dynamical system. The induced *2-norm* of the difference between the *T*-matrices for the two state machines can be used as a measure of anomaly, i.e. $\boldsymbol{M}(\boldsymbol{S},\boldsymbol{S}_0)=\left\|\boldsymbol{T}-\boldsymbol{T}_0\right\|_2$. Such a measure was found to be effective. However, there is some subtlety in using this measure on e-machines, because e-machines do not guarantee that the machines formulated from the symbol sequences $\boldsymbol{S}$ and $\boldsymbol{S_0}$ have the same number of states; and these states do not necessarily have similar physical significance. In general, $\boldsymbol{T}$ and $\boldsymbol{T}_0$ may have different dimensions and different physical significance. However, by encoding the causal states, $\boldsymbol{T}$ could be embedded in a larger matrix, and an induced norm of the difference between $\boldsymbol{T}$ matrices for these two machines can be defined. Alternatively, a (vector) measure of anomaly can be derived directly from the stochastic matrix $\boldsymbol{T}$ as the left eigenvector **p** corresponding to the unit eigenvalue of $\boldsymbol{T}$, which is the state probability vector under a stationary condition.

In the case of *D*-Markov machines, which have a fixed state structure, the state probability vector **p** associated with the state machine have been used for a vector representation of anomalies, leading to the anomaly measure $\boldsymbol{M}(\boldsymbol{S},\boldsymbol{S}_0)$ as a distance function between the respective probability vectors **p** and $\mathbf{p_0}$ (that are of identical dimensions), or any other appropriate functional.

3.3 The BWR Reference Model

The US NRC coupled code TRACE/PARCS is used to generate the time series data. The reference BWR model for this study is based on the Peach Bottom 2 (PB2), for which the TRACE/PARCS models have been validated in the framework of the OECD/NRC BWR TT Benchmark[5]. The plant nodalisation scheme, which served to develop the system input deck of TRACE, is given in Figure 3.3.

The TRACE-inputs decks have been specifically designed to conduct this study. In particular, the control system (Figure 3.4) was provided with capability for different system perturbations. Point kinetics model and three-dimensional kinetics PARCS model were developed to perform either TRACE stand-alone (with point kinetics model) or coupled TRACE/PARCS steady-state and transient simulations.

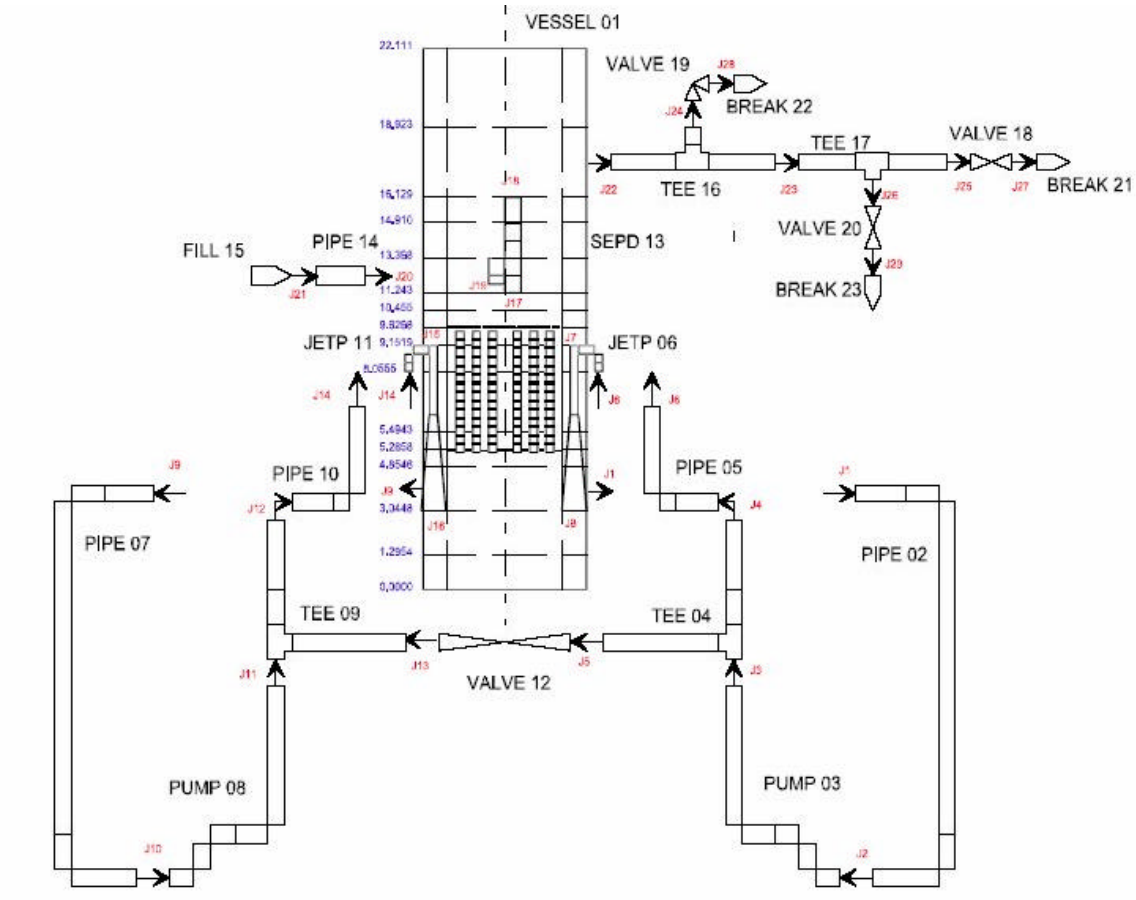

Figure 3.3 PB2 Plant Nodalization

The control system serves a dual purpose: first, it is set up to adjust the plant's relevant parameters to their rated conditions set-points, as reported in Table 3.1; secondly, the control system provides capability for system perturbation. A schematic of the control system is in Figure 3.4.

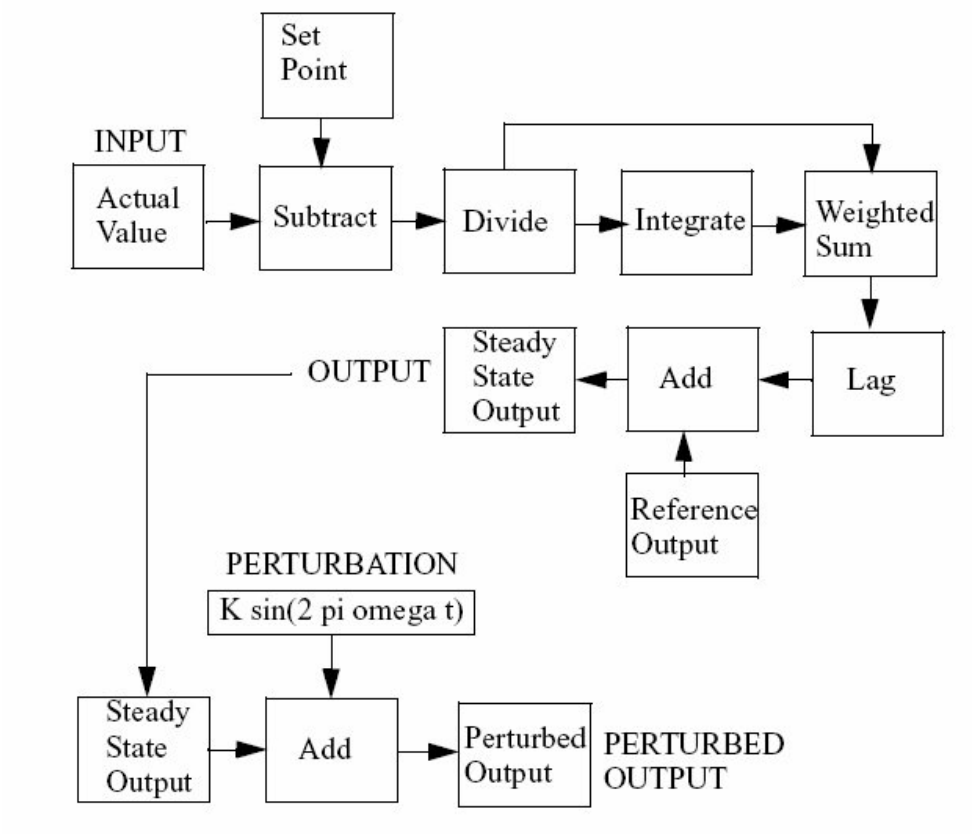

Figure 3.4 Control System Schematic

Table 3.1 BWR Full Power Steady-State Conditions

Thermal Power [MW]	3293
Feedwater / Steam Mass Flow rate [kg/s]	1685
Core Mass Flow rate [kg/s]	12915
System Pressure [MPa]	7.03
Downcomer Water Level [m]	11.2
Core Inlet Subcooling [K]	13

3.4. Selection of Appropriate Input Stimuli

In order to facilitate early detection of small changes in the BWR system parameters that may eventually lead to instabilities, it is proposed to excite the system with opportune *a priori* known stimuli and discover anomaly patterns, if any, from the resulting responses. The study considers BWR system operations in which anomalies do occur at a slow time-scale while the inferences are made based on the observation of the fast time–scale system dynamics. The algorithm of anomaly detection relies on this dual-time scale analysis of the asymptotic response of the dynamical system.

The selection of the set of stimuli to be applied to the system is a critical step for the proposed methodology. The selected perturbation must not interfere with the normal operation of the plant (or, in this case, with the numerical simulation of the plant). In particular, unstable or excessive oscillations must not occur as a consequence of the input perturbations and the plant must return to the original state after the perturbation is terminated. On the other hand, the stimulus imposed to the system has to be ample enough in order for the analyst to infer the stability characteristic of the plant. These observations are especially true for externally applied small perturbations. Four possible types of perturbation have been identified (Table 3.2) for a BWR steady-state operation and applied to PB2:

A. System Pressure perturbation by acting on the Turbine Control Valve (TCV).

B. Core Flow perturbation by acting on the Recirculation Pumps.

C. Sub-cooling perturbation by acting on the Feedwater Pre-heaters

D. Changes in Control Reactivity by Control Rods movement

Among the four possible choices, the System Pressure perturbation seems to be the most viable and secure, whereas for the same reasons the use of the control rods movement seem to be the most impractical and are not hence investigated further.

Table 3.2 Appropriate Input Stimuli.

ID	STIMULUS	EXCITATION	CHARACTERISTICS
A.1	Pressure perturbation by TCV	K·sin (2·p·f·t) (Continuos)	f = 0.4 ÷ 0.6 Hz K= 0.02 ÷ 0.04 MPa
A.2	Pressure perturbation by TCV	K·sin (2·p·f·t) (Time Intervals)	f = 0.4 ÷ 0.6 Hz K= 0.02 ÷ 0.04 MPa Time Intervals ?t1= 0.2 ÷ 10 sec ?t2= 0 ÷ 20 sec
A.3	Pressure perturbation by TCV	Square wave (K, ?t1, ?t2)	K= 0.02 ÷ 0.04 MPa ?t1= 0.2 ÷ 10 sec ?t2= 0 ÷ 20 sec
B.1	Core flow perturbation by Recirculation Pump	K·sin (2·p·f·t) (Continuos)	f = 0.4 ÷ 0.6 Hz K= 0.05% ÷ 0.1%
B.2	Core flow perturbation by Recirculation Pump	K·sin (2·p·f·t) (Time intervals)	f = 0.4 ÷ 0.6 Hz K= 0.05% ÷ 0.1% Time Intervals ?t1= 0.2 ÷ 10 sec ?t2= 0 ÷ 20 sec
B.3	Core flow perturbation by Recirculation Pump	Square wave (K, ?t1, ?t2)	K= 0.05% ÷ 0.1% ?t1= 0.2 ÷ 10 sec ? t2= 0 ÷ 20 sec
C.1	Sub-cooling perturbation by Feedwater Pre-heaters	K·sin (2·p·f·t) (Continuos)	f = 0.4 ÷ 0.6 Hz K= 0.05% ÷ 0.1%
C.2	Sub-cooling perturbation by Feedwater Pre-heaters	K·sin (2·p·f·t) (Time intervals)	2·p·f = 0.4 ÷ 0.6 Hz K= 0.05% ÷ 0.1% Time Intervals ?t1= 0.2 ÷ 10 sec ?t2= 0 ÷ 20 sec
C.3	Sub-cooling perturbation by Feedwater Pre-heaters	Square wave (K, ?t1, ?t2)	K= 0.05% ÷ 0.1% ?t1= 0.2 ÷ 10 sec ?t2= 0 ÷ 20 sec

The control blocks are able to simulate for each of the selected input stimuli, the following three perturbations shapes (Figure 3.5): 1) continuous sinusoidal shape, 2) fragmented sinusoidal shape and 3) square shape.

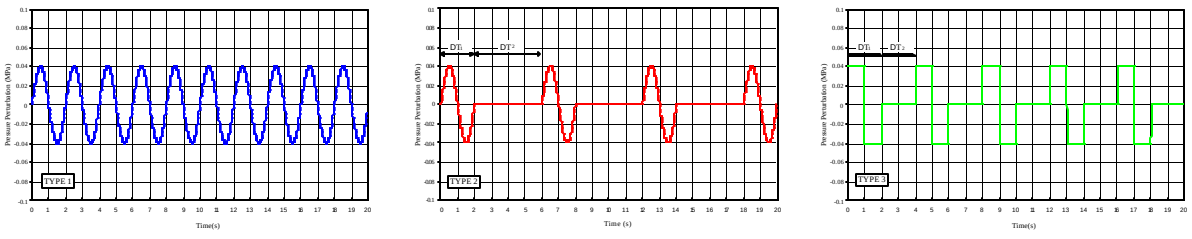

Figure 3.5 Types of Perturbation that Can be Simulated.

Between all these types of stimuli perturbation, the pressure perturbation by acting on the Turbine Control Valve was identified to be the most viable. Linear frequency-domain analyses and operational experience confirm that the typical natural frequency of BWR instability events is about 0.5 Hz. For those reasons, the value of 0.5 Hz is initially chosen for the frequency of system pressure perturbations together with amplitude of 0.02 MPa. Figure 3.6 shows the pressure perturbation applied to the BWR model beginning from a time of 2000 seconds.

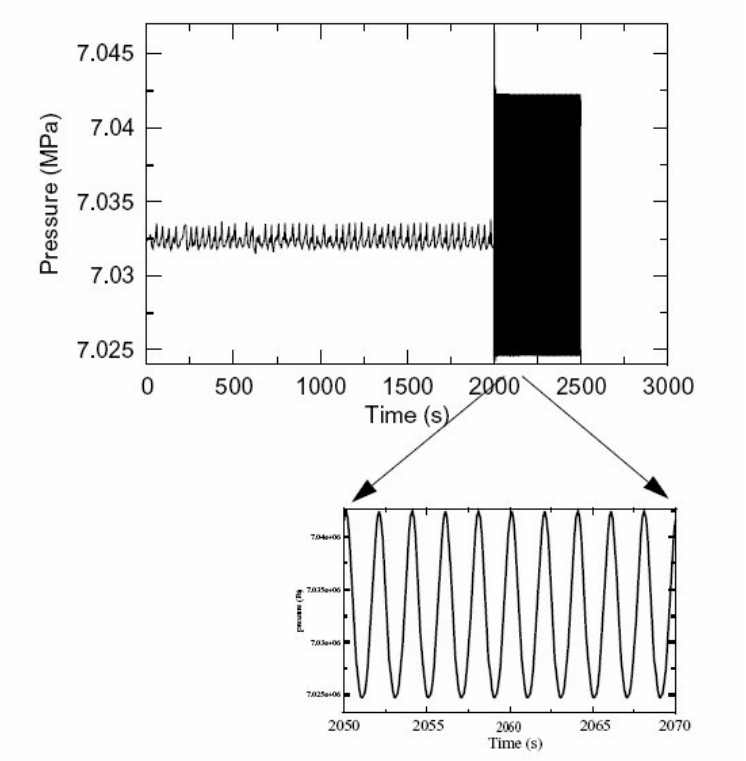

Figure 3.6 System Pressure Perturbation

3.5 Identification of Appropriate Perturbed Parameters

Another critical step of the methodology is the selection of suitable perturbed (possibly slowly) parameters. The followed approach consists in taking into account a combination of the most sensitive stability variables.

Table 3.3 The Most Sensitive Stability Parameters.

PARAMETERS	EFFECT ON STABILITY
Fuel Assembly Parameters	
Flow Area	+
Hydraulic Diameter	+
Loss Coefficient at Lower Tie Plate	+
Loss Coefficient at Upper Tie Plate	-
Loss Coefficient Spacer	-
Fuel Time Constant	+
Void Coefficient	+
Operating Parameters	
Reactor Power Level	+
Reactor Mass Flow	+
Axial Peaking Factor	-
Radial Peaking Factor	-
Inlet Sub-cooling	-/+

Based on the parameters in Table 3.3 an on their relevance to the BWR stability, the following no-dimensional groups of parameters have been used in the anomaly detection methodology:

1) $$b_1 = \frac{P}{M} \cdot \frac{t_f \cdot t_m}{A_m}$$

P = Power (W)
M = Core Mass Flow (Kg/s)
t_f = Fuel Time Constant (s)
t_m = Moderator Time Constant (s)
A_m = Average Core Flow Area (m^2)

- $P \cdot t_f$ = Energy produced in the fuel (J) during the time span t_f in which a change DT_f of the fuel temperature occurs.

- $\frac{M \cdot A_m}{t_m}$ = Energy removed by the coolant during the time span t_m in which a change DT_m of the coolant temperature occurs.

2) $$b_2 = \left| r_a \cdot a \right|$$

r_a = Reactivity Void Coefficient (1/%void)
a = Average Core Void (%void)

- Insertion of void reactivity

3) $$b_3 = \frac{\left| r_a \cdot a \right|}{\left| r_T \cdot T \right|}$$

r_T = Reactivity Temperature Coefficient (1/T)
T = Average Core Temperature (T)

- $r_a \cdot a$ = Insertion of reactivity from Void Effect
- $r_T \cdot T$ = Insertion of reactivity from Doppler Effect
- Importance of the reactivity effects

4) $$b_4 = \frac{p_{avg}}{\Delta p}$$

p_{avg} = Core Average Pressure
Dp = Core Pressure Drop

- Effect of pressure drops.

5) $$b_5 = \frac{h_l^{sat} - h_l}{h_g^{sat} - h_{ll}^{sat}}$$

h_l = Inlet Liquid Enthalpy
h_l^{sat} = Liquid Enthalpy at T_{sat}
h_g^{sat} = Vapour Enthalpy at T_{sat}

- Effect of subcooling degree.

6) $$b_6 = \frac{P}{M} \cdot \frac{r_l^{sat} - r_g^{sat}}{r_g^{sat}} \cdot \frac{1}{h_g^{sat} - h_l^{sat}} = NPCH$$

NPCH = Phase Changing Number

r_l^{sat} = Liquid Density at T_{sat}

r_g^{sat} = Vapour Density at T_{sat}

7) $$b_7 = \frac{h_l^{sat} - h_l}{h_g^{sat} - h_{ll}^{sat}} \cdot \frac{r_l^{sat} - r_g^{sat}}{r_g^{sat}} = NSUB$$

NSUB = Subcooling Number

8) $$b_8 = b_3 \cdot \frac{t_m}{t_f} = \frac{|r_a \cdot a|}{|r_T \cdot T|} \cdot \frac{t_m}{t_f}$$

- Importance of the reactivity effects taking into account the different time constants.

9) $$b_9 = b_1 \cdot b_3 = \frac{P}{M} \cdot \frac{t_f \cdot t_m}{A_m} \cdot \frac{|r_a \cdot a|}{|r_T \cdot T|}$$

In particular parameters ß$_1$, ß$_3$, ß$_4$ and ß$_6$ were identified to be more viable to detect difference in the asymptotic behavior by slow and small changes in their values (see the following Sections).

3.6 Generation of Time Series Data

The US NRC thermal-hydraulic system code TRACE (TRAC RELAP Advanced Computation Engine) coupled with the 3-D neutronics simulator PARCS is used to simulate the Peach Bottom 2 NPP. Initially the point kinetics model, implemented in TRACE, is used to simulate the thermal-hydraulics/neutron kinetics feedbacks. This model is sufficient to predict the in-phase instabilities. However, the 3-D kinetics model (PARCS) has already been developed and applied in order to:

1) predict the out-of phase instabilities, and

2) refine the model to predict the in-phase instability

Tree different scenarios, based on the different dependence of the reactivity void coefficient on the core average exposure, were simulated (Figure 3.7):

a. BOL: Beginning of Life or Beginning of Cycle (BOC);

b. EOL: End of Life or End of Cycle (EOC)

c. CC1: Conservative Case 1 (more insertion of reactivity due to the void feedback effect)

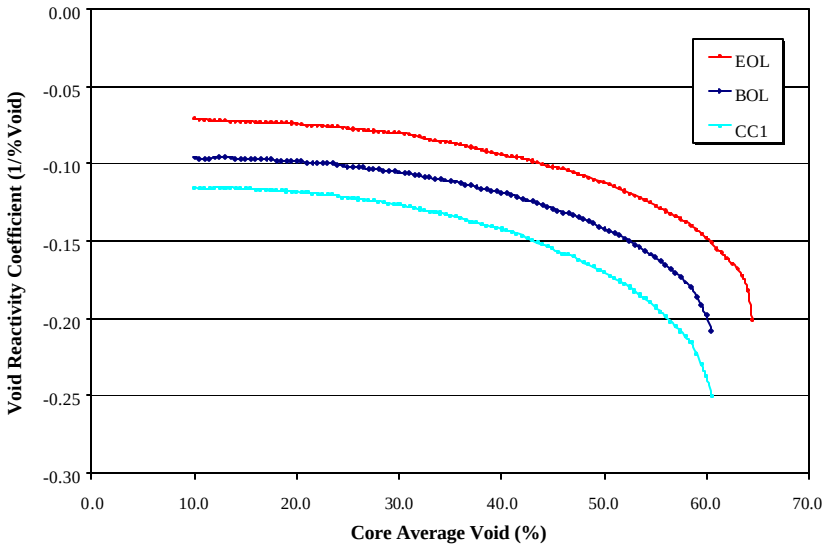

Figure 3.7 Void Reactivity Coefficients as a Function of the Average Core Void

For each scenario, a set of simulations have been performed starting from the rated condition (100% Power, 100% Mass Flow Rate) and moving along the Operational Map of the PB NPP (Figure 3.8 and Table 3.4). For each of these calculations, sensitivity studies have been performed changing some parameters in Table 3.3 (Inlet Sub-cooling, Loss Coefficient at Lower Tie Plate, etc). Results of the simulations have been used to calculate the beta parameters for the anomaly curves (see Section 3.7).

After 2000 seconds of "null" transient simulation, the pressure perturbations, described in Section 3.4 are applied for 500 seconds. The identification of small changes in the behavior of nonlinear dynamics systems requires the selection of appropriate time series data. The following ones have been taken into considerations:

a. Core Mass Flow In, Core Mass Flow Out;

b. Reactor Power;

c. Void Reactivity Feedback, Doppler Reactivity Feedback;

d. Cladding Rod Temperature;

e. Feed Water Flow Rate, Steam Line Flow rate;

f. Feed Water Temperature, Core Inlet Temperature, Subcooling Degree;

g. RPV Downcomer Level;

h. Steam Dome Pressure;

i. NSUB and NPCH

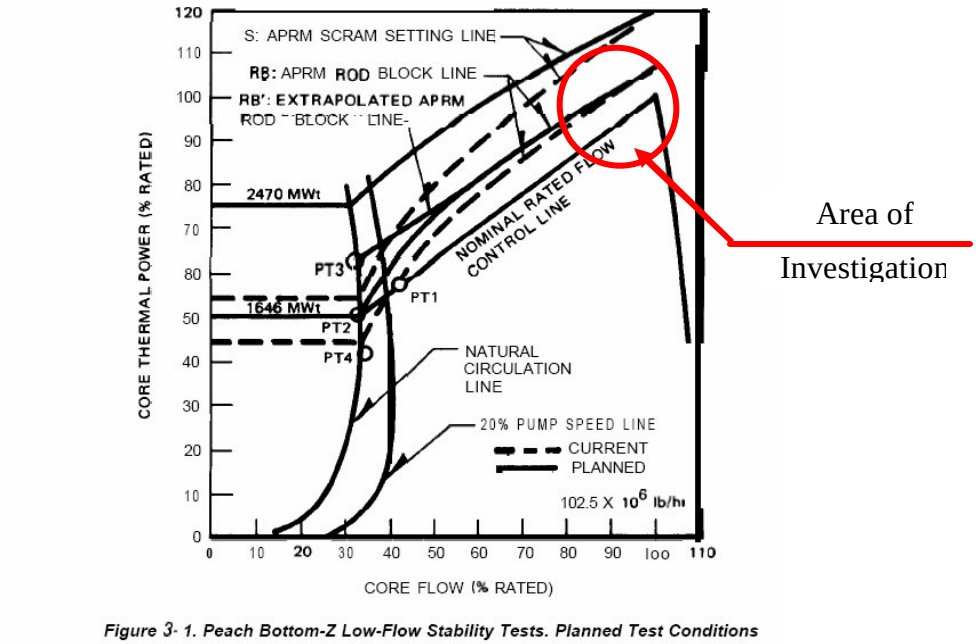

Figure 3- 1. Peach Bottom-Z Low-Flow Stability Tests. Planned Test Conditions

Figure 3.8 PB2 Operational Map.

Table 3.4 List of calculations obtained by varying power (P) and Mass Flow Rate (M)

Nominal Power (100%) = 3293000 W
Nominal Core Flow (100%) = 12915 Kg/s

P = 50 + (50/65)*(M-35)

N°	M (%)	P (%)	P(%)/M(%)	M (Kg/s)	P (kW)	P/M (kJ/Kg)
1	**100.0**	100.00	1.000	12915	3293000	254.97
2	**99.5**	99.62	1.001	12865.33	3280335	255.27
3	**99.0**	99.23	1.002	12815.65	3267669	255.57
4	**98.5**	98.85	1.004	12765.98	3255004	255.87
5	**98.0**	98.46	1.005	12716.31	3242338	256.18
6	**97.5**	98.08	1.006	12666.63	3229673	256.48
7	**97.0**	97.69	1.007	12616.96	3217008	256.79
8	**96.5**	97.31	1.008	12567.29	3204342	257.11
9	**96.0**	96.92	1.010	12517.62	3191677	257.43
10	**95.5**	96.54	1.011	12467.94	3179012	257.75
11	**95.0**	96.15	1.012	12418.27	3166346	258.07
12	**94.5**	95.77	1.013	12368.6	3153681	258.40
13	**94.0**	95.38	1.015	12318.92	3141015	258.73
14	**93.5**	95.00	1.016	12269.25	3128350	259.07
15	**93.0**	94.62	1.017	12219.58	3115685	259.40
16	**92.5**	94.23	1.019	12169.9	3103019	259.75
17	**92.0**	93.85	1.020	12120.23	3090354	260.09
18	**91.5**	93.46	1.021	12070.56	3077688	260.44
19	**91.0**	93.08	1.023	12020.88	3065023	260.79
20	**90.5**	92.69	1.024	11971.21	3052358	261.15
21	**90.00**	92.31	1.026	11623.5	3039692	261.51

In particular **Core Mass Flow Out, NPCH**, **Power** and **Steam Dome Pressure** have been investigated in depth. Figures 3.9, 3.10, 3.11 and 3.12 show respectively the above mentioned time series data for the BOL scenario during the selected pressure perturbation transients starting (after 2000 s) from some of the considered conditions above in Table 3.4.

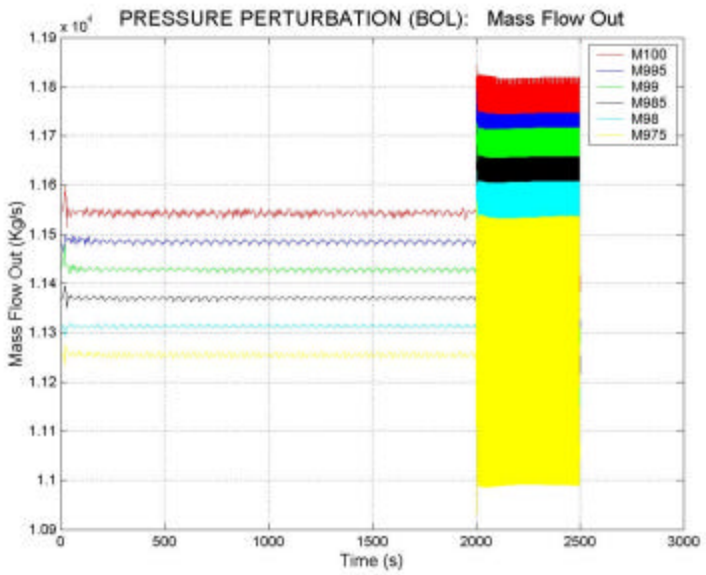

Figure 3.9 Mass flow out time trend during the pressure perturbation transient for BOL scenario and different steady state conditions.

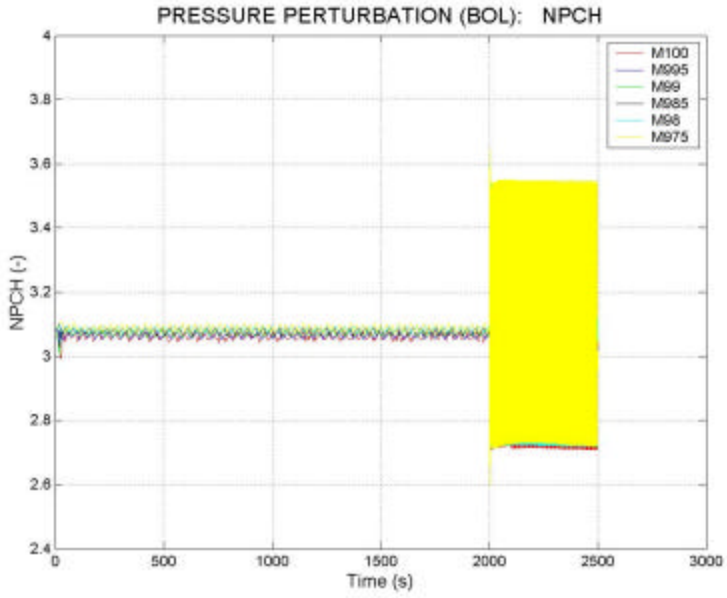

Figure 3.10 NPCH time trend during the pressure perturbation transient for BOL scenario and different steady state conditions.

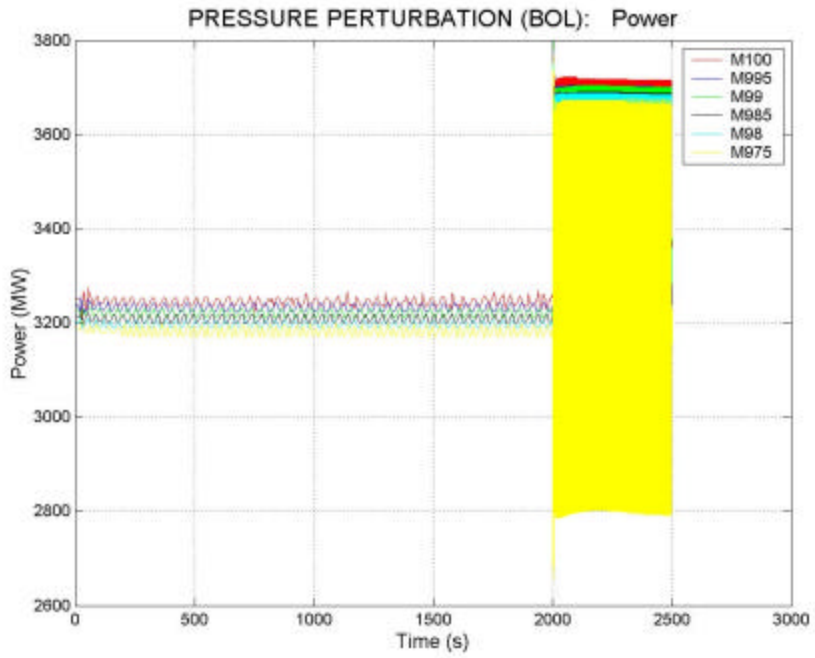

Figure 3.11 Mass flow out time trend during the pressure perturbation transient for BOL scenario and different steady state conditions.

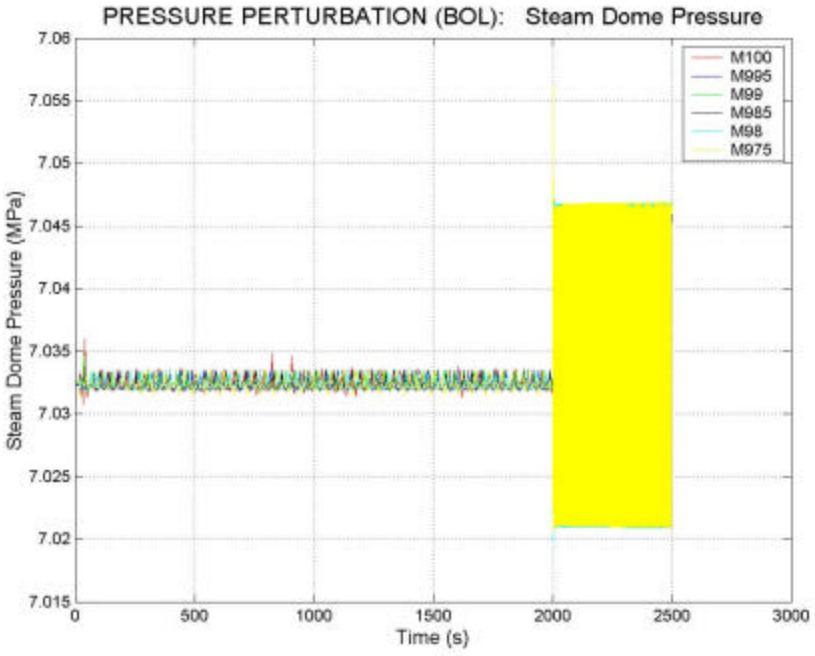

Figure 3.12 Steam Dome Pressure time trend during the pressure perturbation transient for BOL scenario and different steady state conditions.

3.7 Results from the Application of Early Anomaly Detection of BWR Instabilities

The combination of Symbolic Dynamics and Formal Languages provides a tool for identification of small changes in the behavior of nonlinear dynamical systems. The transition from the continuous to a discrete symbolic description is accomplished by choosing a suitable Poincare section for the time discretization. The resulting phase-space of the dynamical system is partitioned into a number of cells to generate a "coordinate grid". Each cell is labeled with a symbol and the set of all such symbols constitutes the "alphabet" of the symbolic dynamics. Such a mapping attributes a legal (physically admissible) symbol sequence to the system dynamics starting from the initial state, as the dynamic trajectory in the phase-space is represented by legal strings of symbols (symbolic language). The phase-space plots reported in Figures 3.13, 3.14, and 3.15 constitute examples of the graphs used to generate the symbol sequences. They refer to the BOL scenario with different conditions ranging from 100% of mass flow rate and power to 90% of mass flow and 92.31% of power. In particular, it is possible to note the change of the orbit's shapes for the following 2-dimensional phase space:

a. Mass Flow In versus Mass Flow Out;

b. Core Power versus NPCH;

c. Power versus Mass Flow In.

The construction procedure for ϵ machines is based upon the translation of the string of symbols into a parse tree. A probabilistic structure is then added to each tree node in such a way that the transition probabilities between different system states (upon occurrence of each symbol of the alphabet) can be determined and represented by a (stochastic) connection matrix T, which is denoted as a vector representing any possible anomaly in the dynamical system. An appropriate norm of the difference between the matrices T under nominal and anomalous conditions is used in the investigation as a measure of anomaly.

Figures 3.16 through 3.19 show the results obtained by the application of the early anomaly detection of BWR instabilities respectively for BOL and EOL. Similar results have been obtained for the conservative case CC1. For each scenario, two time series data have been considered (Mass Flow Out and NPCH) and for each of them four different beta parameters have been adopted. The behavior is substantially the same for all graphs and three different regions can be identified:

1) a first zone where the anomaly curves increases quite rapidly outlining the features of early anomaly detection methodology;

2) a plateau region that corresponds to the 'critical' combination of parameters;

3) a third zone where the anomaly curves restarts to increases, identifying the possible incoming BWR instabilities.

For example in the anomaly curve for the case of BOL in which the Mass Flow Out time series data was analyzed using the proposed anomaly detection methodology to detect growth of anomaly as parameter $ß_1$ increases, one can see a rapid rise in anomaly measure from the nominal $ß_1$ value. This indicates that the technique is successful in detecting early growth in anomaly. The anomaly curve starts to level on at $ß_1 = 2.65 \times 10^5$ and starts to slightly increase again at a $ß_1$ value of approximately 2.88×10^5, which might indicate incoming BWR instabilities.

Each anomaly curves is bounded with uncertainty bands with a confidence level of 98%. The uncertainty bands are created from calculating the prediction bounds. The prediction bounds can be calculated for a new observation or for the fitted function. In creating our uncertainty bands, we calculated prediction bounds for the fitted function. Additionally, the bounds can be simultaneous and measure the confidence for all predictor values or non-simultaneous and measure the confidence only for a single predetermined predictor value. A simultaneous bound was used with a confidence level of 0.98, which indicates a 98% level of certainty that all predictor values are contained within the lower and upper prediction bounds.

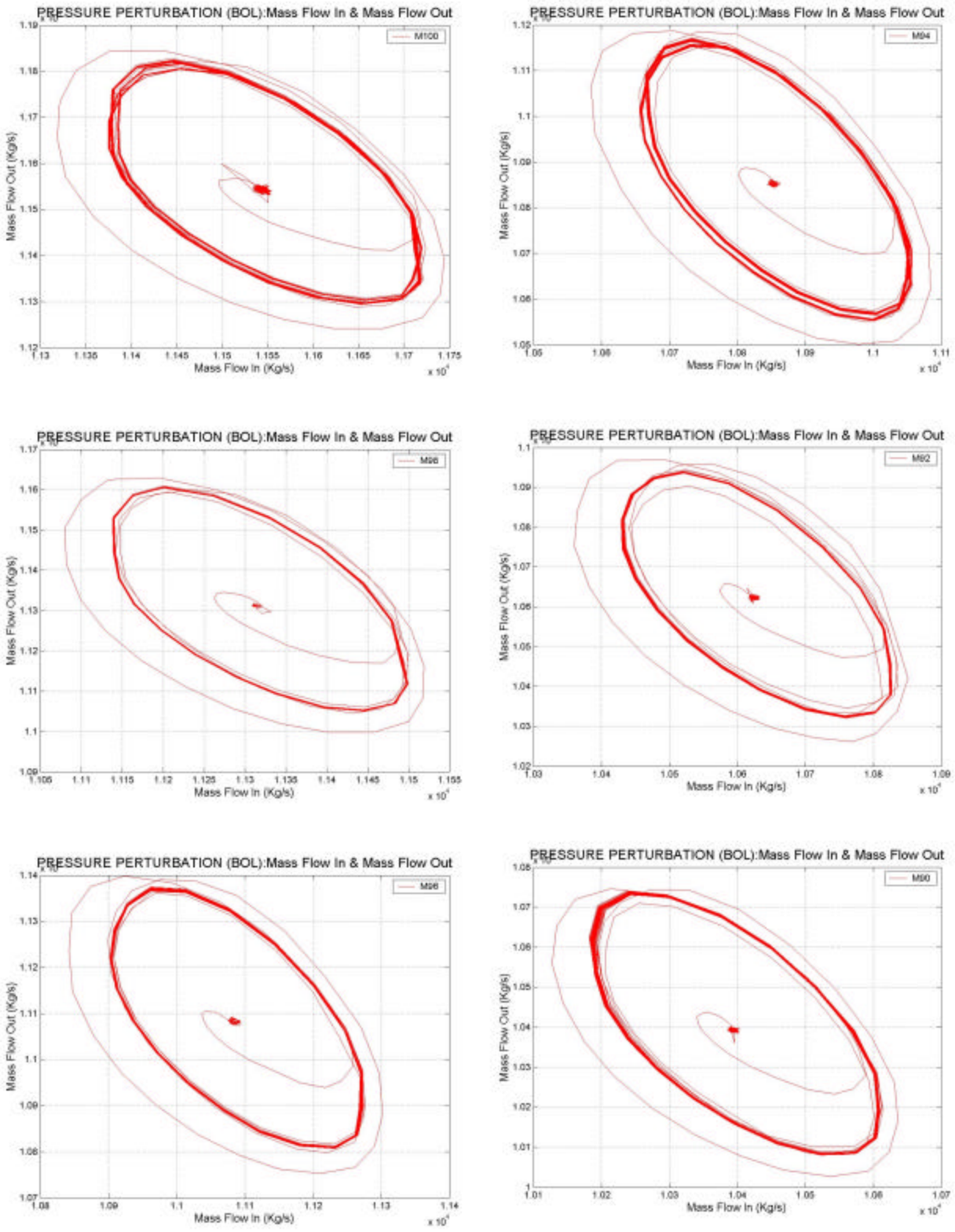

Figure 3.13 Mass Flow In versus Mass Flow Out phase space description: pressure perturbation transient for BOL scenario and different steady state conditions.

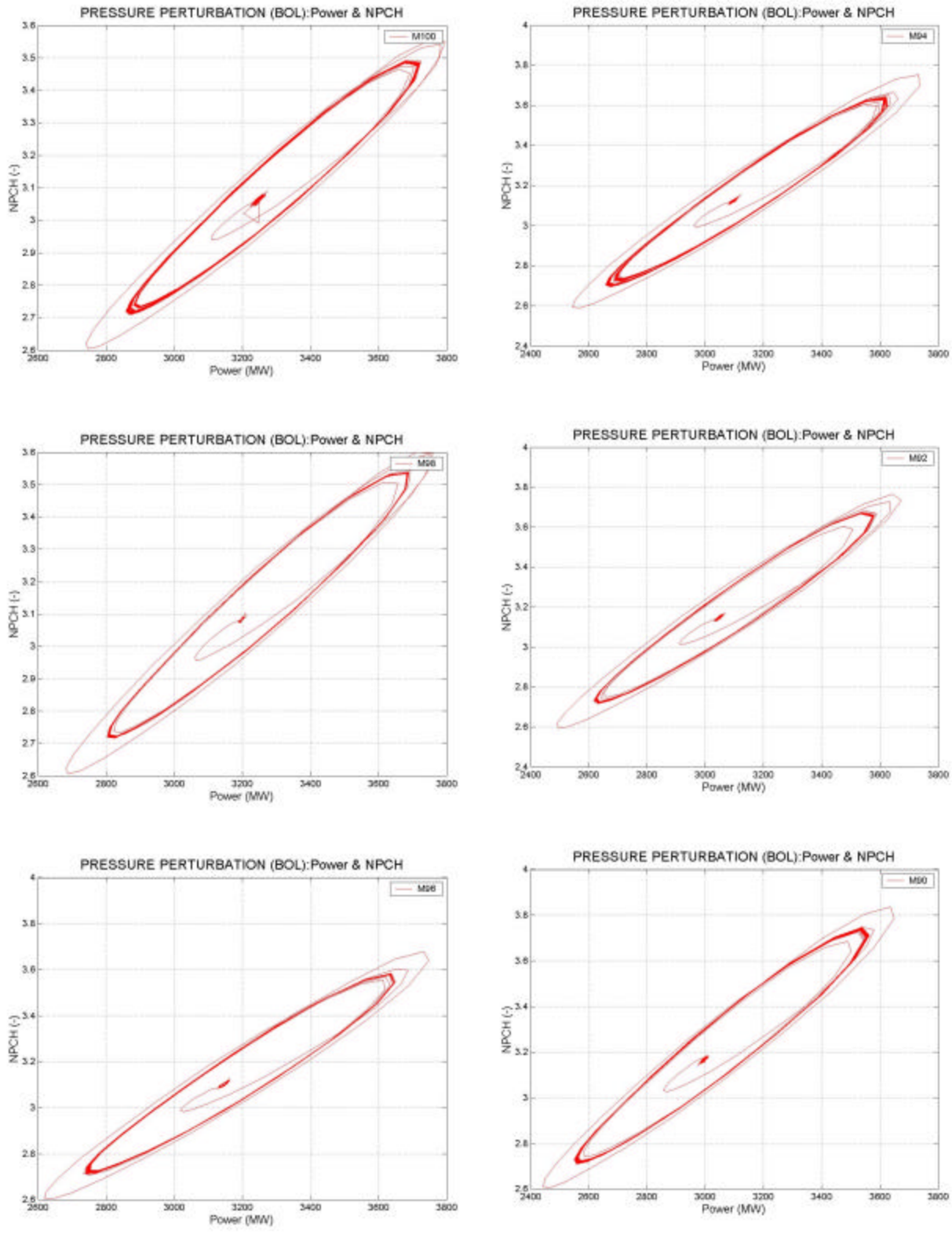

Figure 3.14 NPCH versus Power phase space description: pressure perturbation transient for BOL scenario and different steady state conditions.

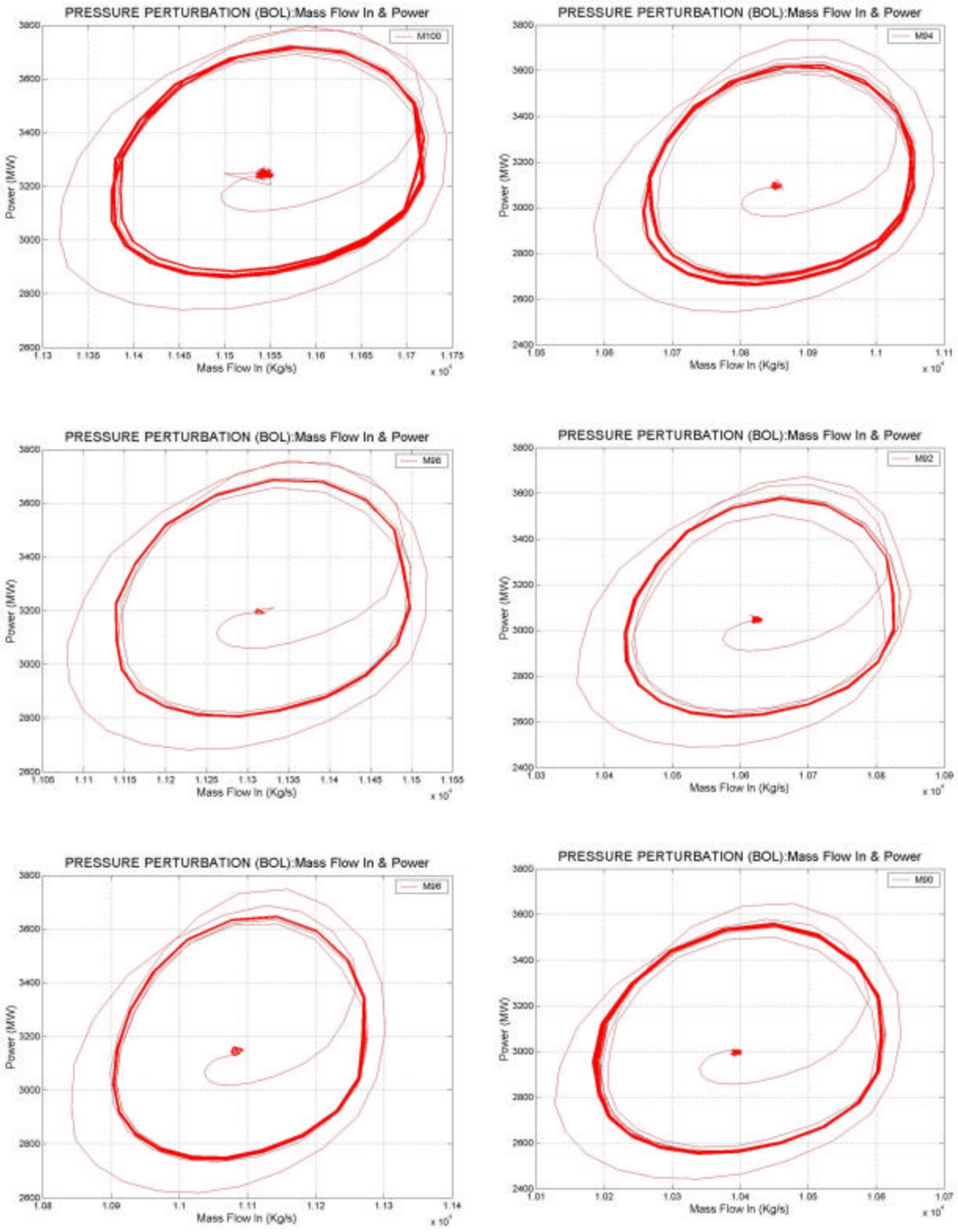

Figure 3.15 Power versus Mass Flow In phase space description: pressure perturbation transient for BOL scenario and different steady state conditions.

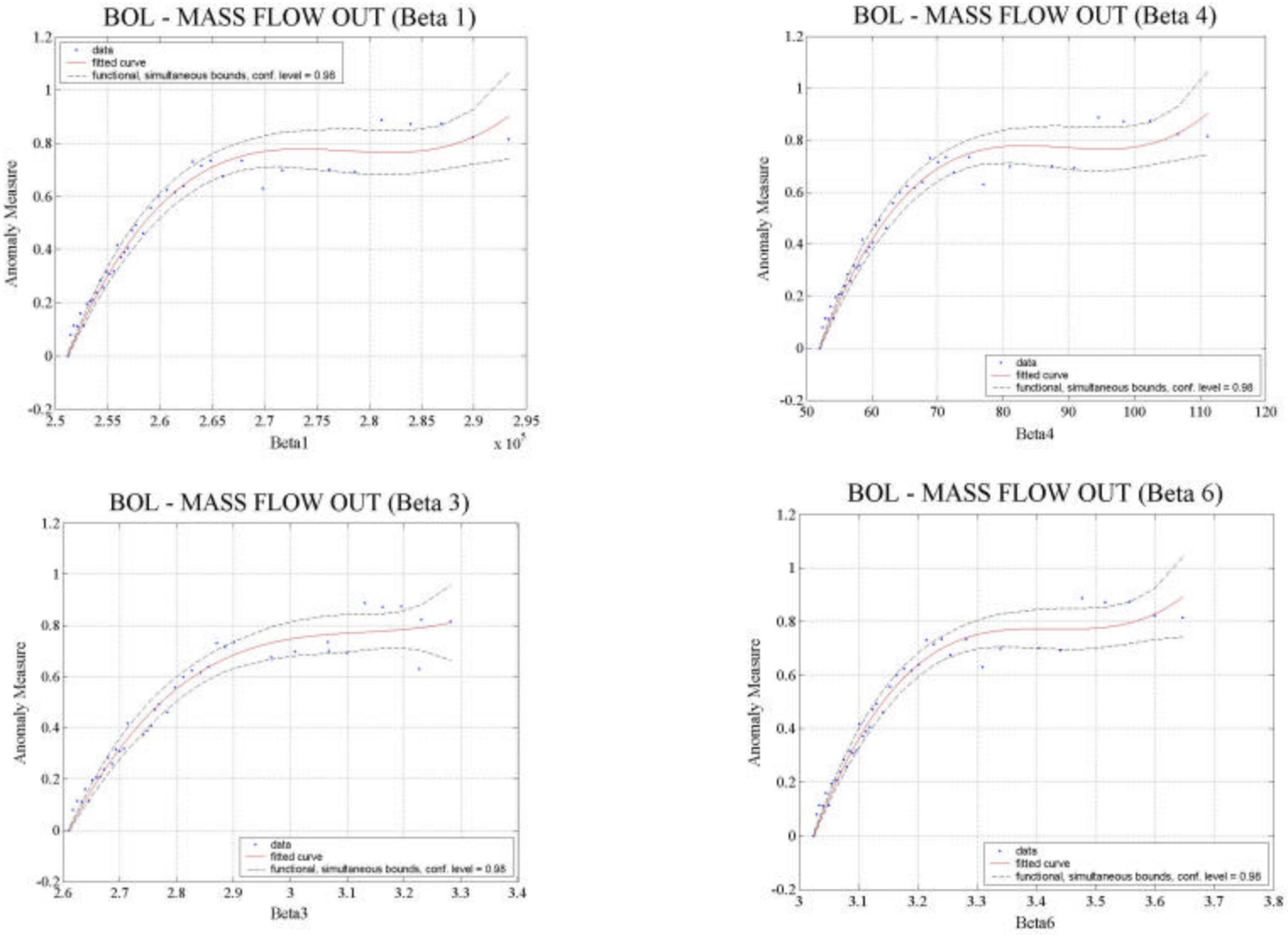

Figure 3.16 Anomaly curves and uncertainty bands. Scenario: BOL – Time Series Data: Mass Flow Out – Parameters: ß$_1$, ß$_2$, ß$_3$ and ß$_4$.

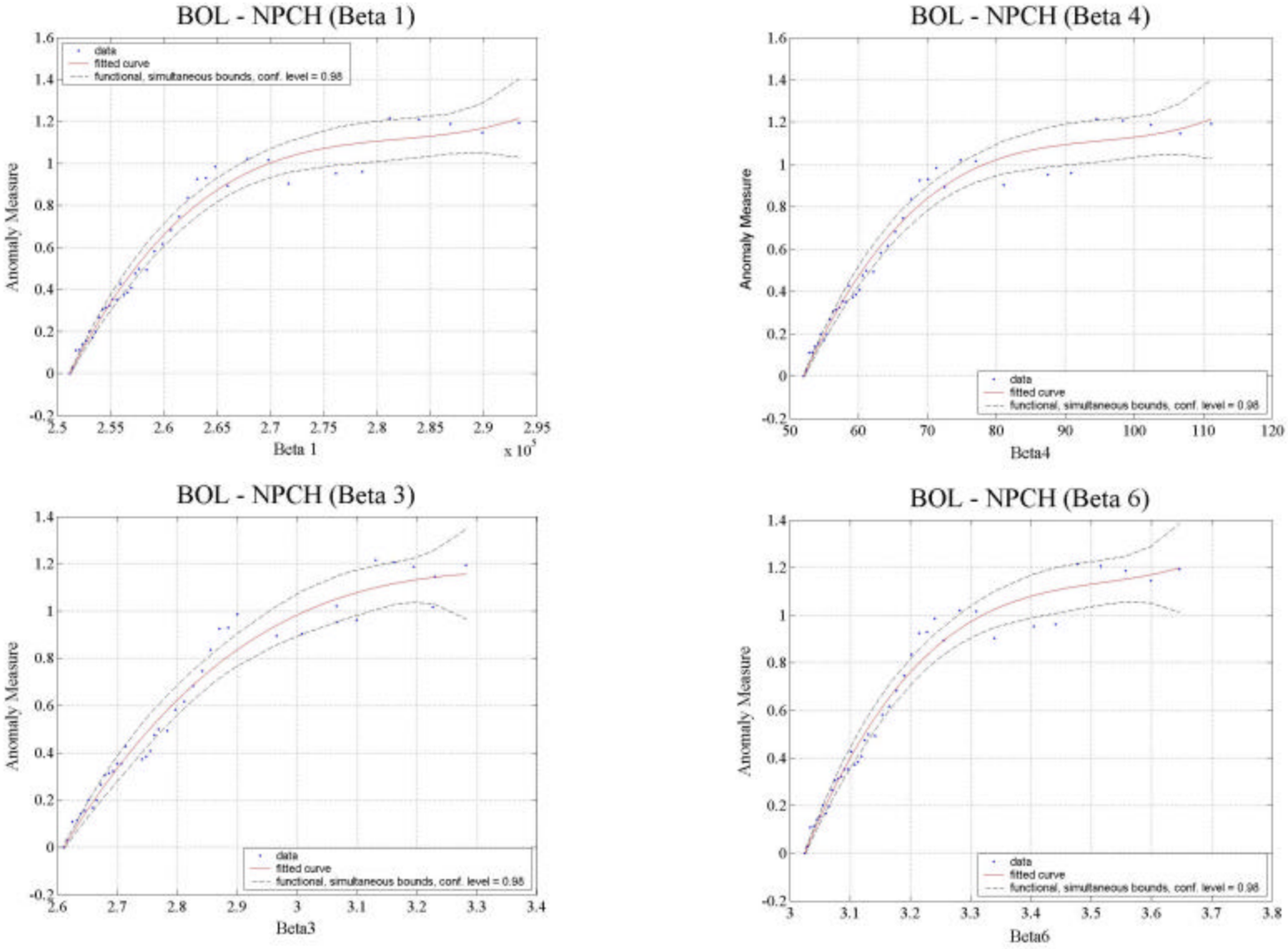

Figure 3.17 Anomaly curves and uncertainty bands. Scenario: BOL – Time Series Data: NPCH – Parameters: $ß_1$, $ß_2$, $ß_3$ and $ß_4$.

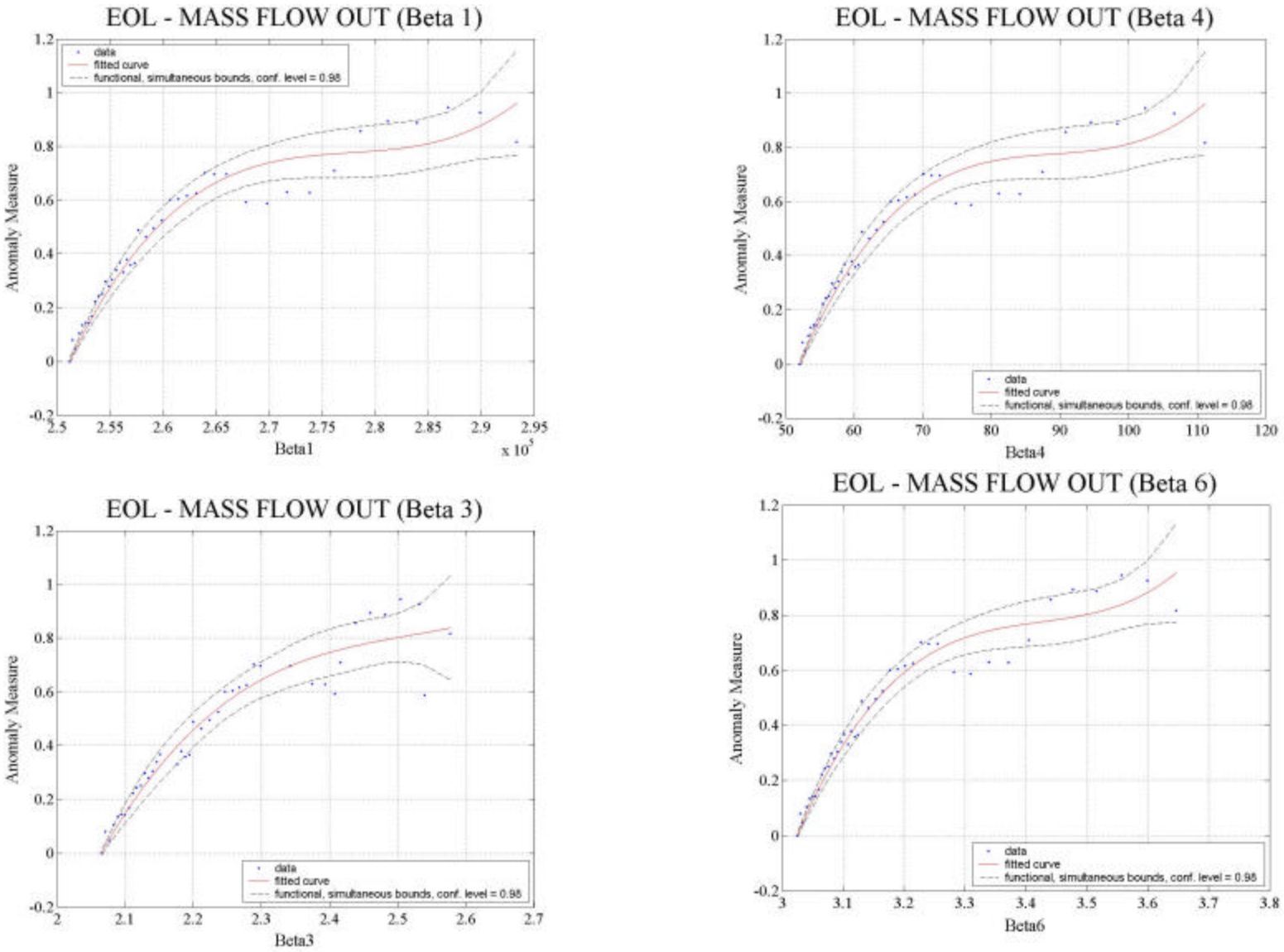

Figure 3.18 Anomaly curves and uncertainty bands. Scenario: EOL – Time Series Data: Mass Flow Out – Parameters: ß$_1$, ß$_2$, ß$_3$ and ß$_4$.

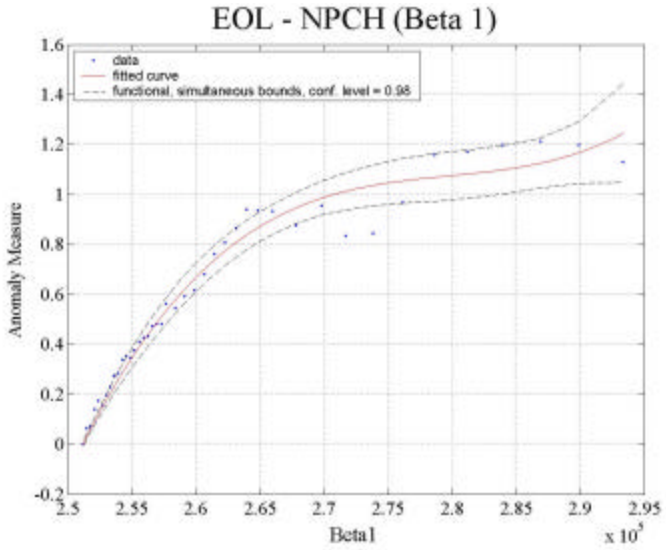
EOL - NPCH (Beta 1)
data
fitted curve
functional, simultaneous bounds, conf. level = 0.98
Anomaly Measure
Beta1
x 10^5

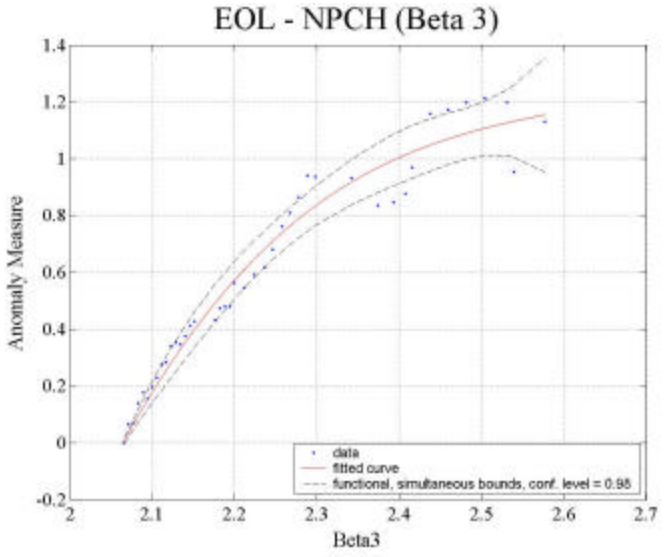
EOL - NPCH (Beta 3)
data
fitted curve
functional, simultaneous bounds, conf. level = 0.98
Anomaly Measure
Beta3

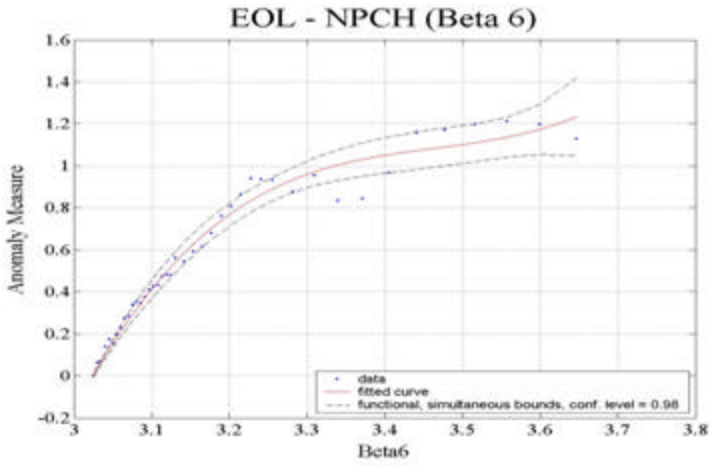
EOL - NPCH (Beta 6)
data
fitted curve
functional, simultaneous bounds, conf. level = 0.98
Anomaly Measure
Beta6

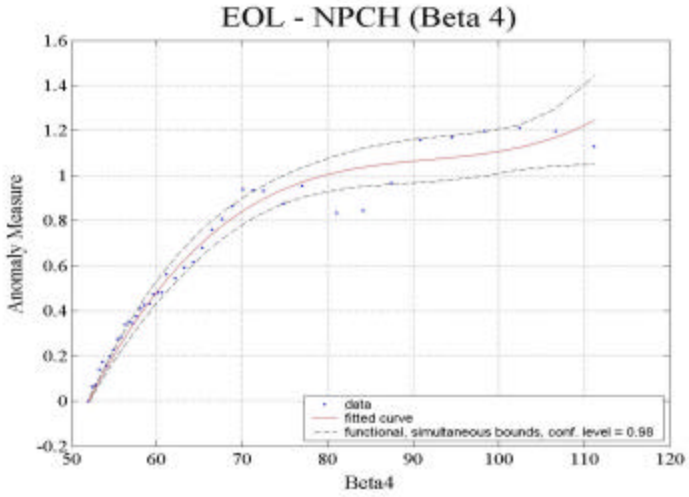
EOL - NPCH (Beta 4)
data
fitted curve
functional, simultaneous bounds, conf. level = 0.98
Anomaly Measure
Beta4

Figure 3.19 Anomaly curves and uncertainty bands. Scenario: EOL – Time Series Data: NPCH – Parameters: ß$_1$, ß$_2$, ß$_3$ and ß$_4$.

3.9 Demonstration of the Capability to Detect BWR Instabilities

It is well known that the BWR operation at rated conditions is always in the stable region, whereas instability events may occur at low flow and relatively high power operation (Figure 3.20).

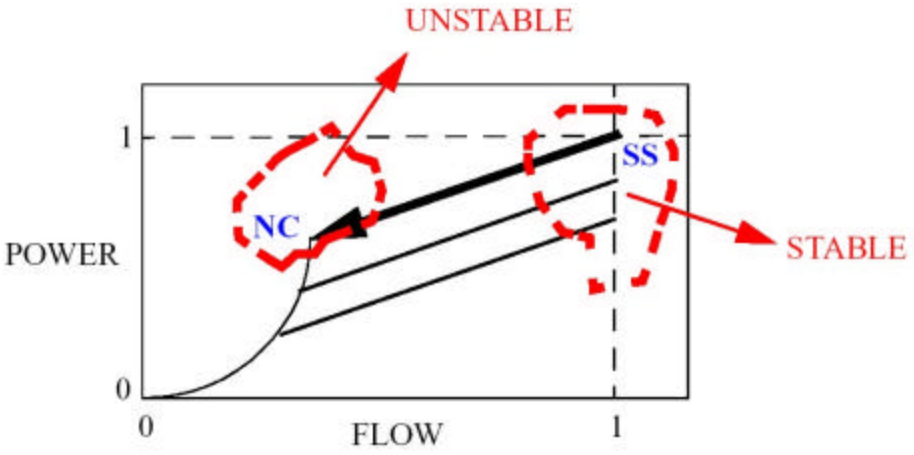

Figure 3.20 BWR Operational Map.

Taking example from the instability accident that occurred at the LaSalle BWR, a series of TRACE simulation of a double recirculation pump trip transient originating at different 'steady state' conditions is executed to determine whether or not instabilities will occur during operation in natural circulation following the pumps trip.

This discussion is intended as a demonstration of the capability of the methodology to predict the BWR instabilities. A more sophisticated qualification process for the proposed methodology is under way and it will constitute one of the main goals to be achieved during the second year of the project.

The analysis presented in this report is focused only on the BOL scenario. Similar results have been obtained for EOL and CC1 scenarios. The base-case simulation (100% of Power and 100% of Mass Flow Rate) shows that the natural circulation mode is stable (Figure 3.21). The re-circulation pump trip occurs at 2000 seconds into the simulation. Subsequent sensitivity calculations show, as expected, that the reactor operation moves towards an unstable behaviour when the insertion of reactivity due to the void feedback increases. In correspondence of 68% of Mass Flow Rate and 75% of Power the first insurgence of instabilities occurs (Figure 3.22). The average core void is 48% and the ß$_3$ parameter has a value of about 3.2. Figure 3.23 shows that in correspondence of this value of ß$_3$ the anomaly measure is 0.78 (the time series data taken into consideration is the Mass Flow Out) and this point is situated in the third zone of the anomaly curves after the plateau region, i.e. where the anomaly methodology identifies the possible presence of BWR instabilities.

In this research, a new methodology for early detection of BWR instabilities has been developed and an initial demonstration of the capability of the methodology to predict the BWR instabilities has been done. A more sophisticated qualification process for the proposed methodology is under way and it will constitute one of the main goals to be achieved during the second year of the NEER project.

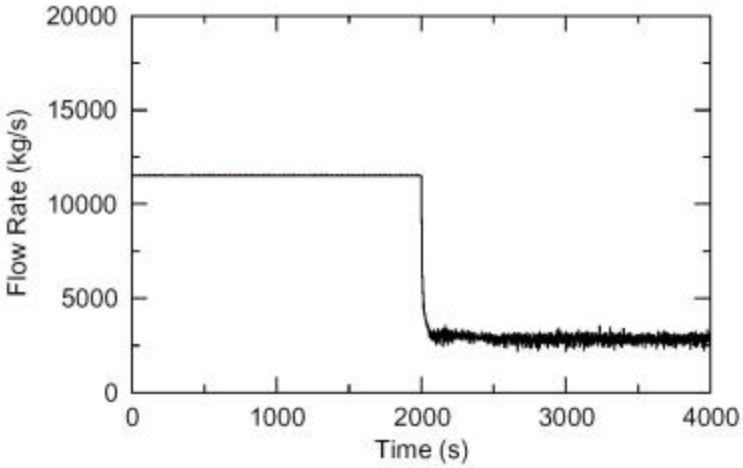

a - Core Flow In

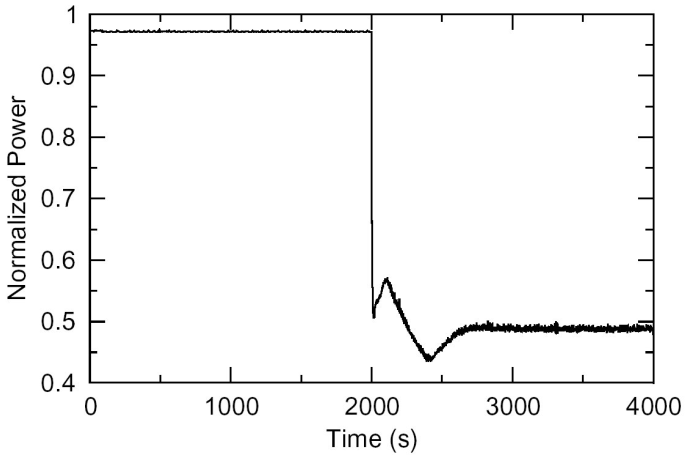

b - Reactor Power

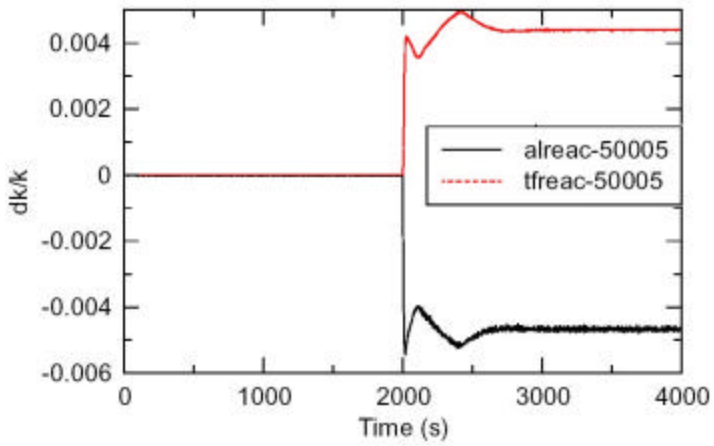

c - Reactivity Components

Figure 3.21 Recirculation Pump Trip: Base-Case.

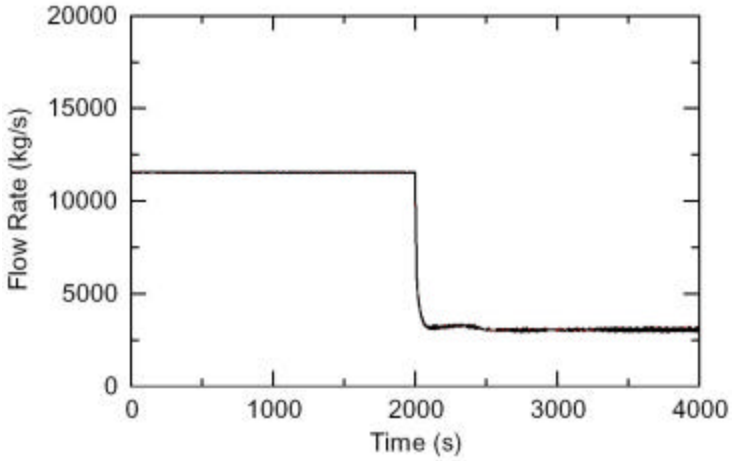

a - Core Flow In

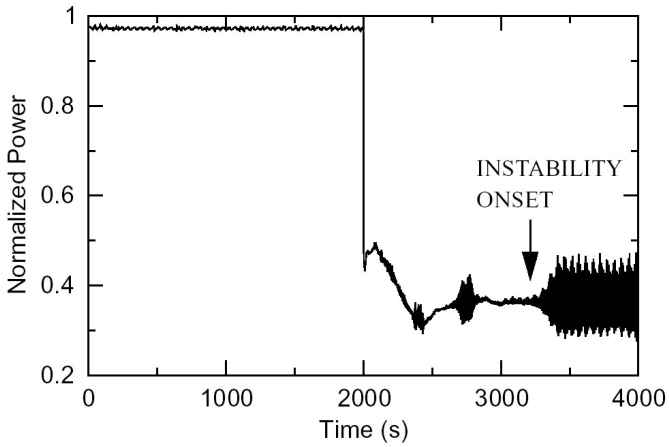

b - Reactor Power

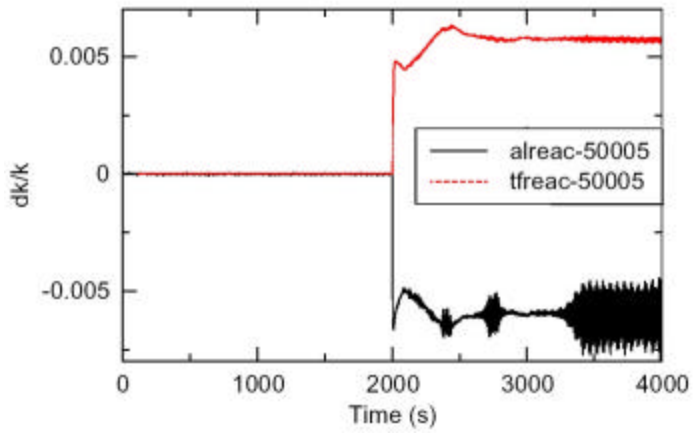

c - Reactivity Components

Figure 3.22 Recirculation Pump Trip: Instability Insurgence for 68% of Mass and 75% of Power

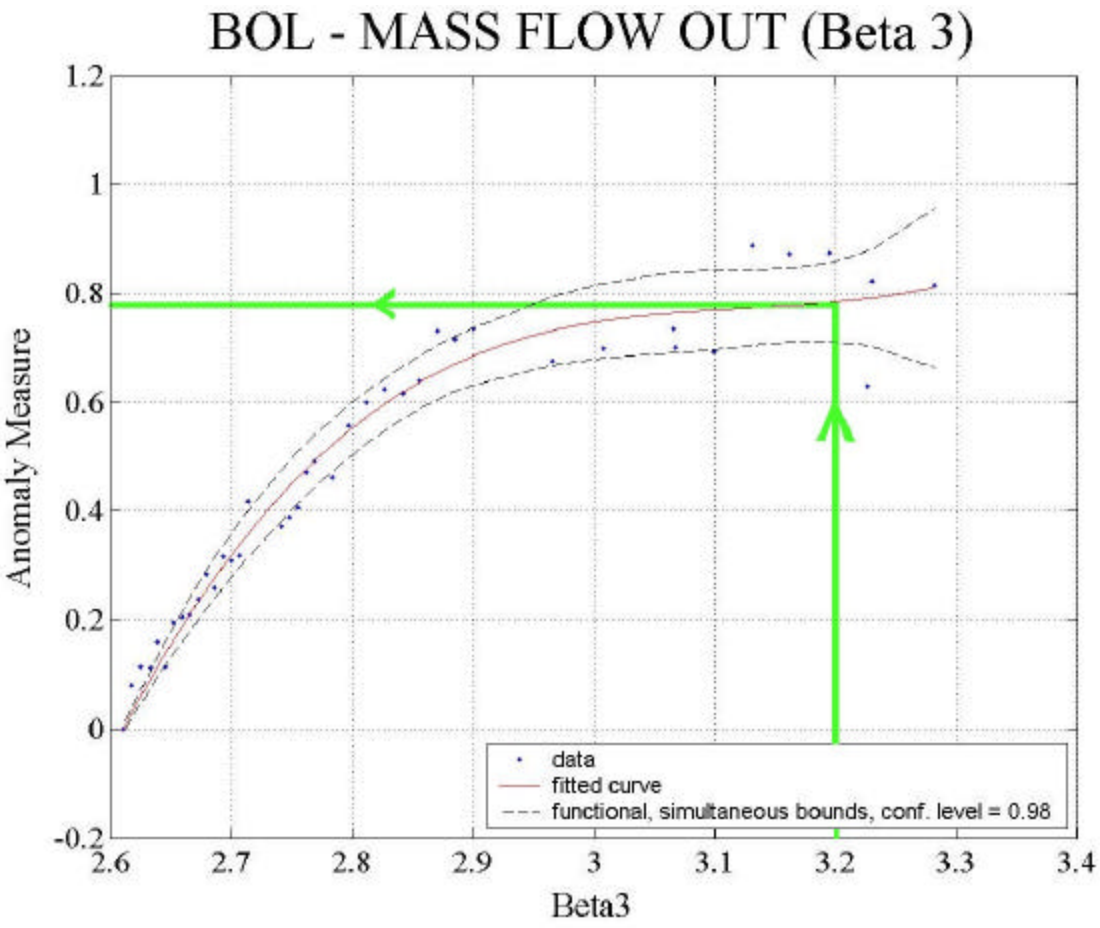

Figure 3.23 Demonstration of the Capability to Detect BWR Instabilities.

4 Project Schedule and Management

The work during the 1st year of the project was performed by Professor Ivanov (as lead principal investigator – PI) and assisted by one Ph.D. student from the Nuclear Engineering Program. The methodology being developed in the framework of the project serves as the PhD dissertation topic of this student. Two other faculty form the MNE Department at PSU, which are members of his PhD Committee, participated actively in this project as non-paid collaborators and advisers. Professor A. Ray is bringing to the project his expertise in system dynamics and artificial intelligence and Professor F. B. Cheung is bringing to the project his expertise in thermal-hydraulics and nuclear safety. The outlined below four Tasks for the Phase 1 of Year 1 of the project are completed.

1) Phase 1 - Year 1:

Task 1 – 3 months (Completed)
Identification of the appropriate stimuli class for BWR-type of instabilities for both simulation models using the coupled simulation tools

Task 2 – 3 months (Completed)
Development of solution procedure for generating time-series data from the models developed under both normal and selected anomaly conditions

Task 3 – 3 months (Completed)
Development of a procedure for conversion from continuous dynamics of time series data to symbolic dynamics.

Task 4 – 3 months (Completed)
Construction of a vector space of formal languages and a metric to serve as a distance function.

The performed work during the first year is summarized in this report and presented to DOE. Two publications are completed based on the accomplished work during the 1st year of the project – one on the concept of the methodlogy[3] and the other on the development of the methdology[6]. A journal paper summarizing the work done during the first year of this project is being finalized and it will be sent to *Annals of Nuclear Energy* for publication.

According to the project schedule the following fours tasks will be performed during he 2nd year of the project.

2) Phase 2 – Year 2:

Task 5 – 2 months
Formulation of a forward functional relationship of the anomalies to the measured distances between symbolic languages under each of the exogenous stimuli

Task 6 – 2 months

Verification of the forward methodology using the simulation models and tools

Task 7 – 3 months
Applications of the Forward Problem Formulation to BWR Instabilities Analyses

Task 8 – 5 Months
Feasibility study on identification of a set of potential anomalies as an intersection of the inverse images of the measured distances between symbolic languages under the forward functional relationship for each of the exogenous stimuli

The performed work during the second year will be summarized in a report and presented to DOE. The performed work on the whole project will be summarized in a final report and presented to DOE. A conference and/or journal paper will be prepared describing the developed methodology and obtained results.

5 Bibliography

1. F. Odar et al, "TRACE V4.0 User's Manual", US NRC, 2003.

2. H. Joo et al, "User's Guide for PARCS", US NRC, 2000.

3. C. Delfino, A. ray, K. Ivanov, and B. Cheung, "A New Concept for Early Detection of BWR Instabilities", TANSAO 88, pp. 292-294, 2003.

4. A. Ray, "Symbolic Dynamic Analysis of Complex Systems for Anomaly Detection", Signal Processing, Vol. 84, No. 7, pp. 1115-1130, 2004.

5. D. Lee, T. Downar, B. Akdeniz, K. Ivanov, and T. Ulses, "Analysis of the OECD/NRC Turbine Trip Transient Benchmark with Coupled Neutronics and Thermal-Hydraulics Code TRAC-M/PARCS", Proceedings of PHYSOR 2002, Korea.

6. A. Petruzzi, S. Chin. K. Ivanov, A. Ray, and B. Cheung, "Development of Methodology for Early Detection of BWR Instabilities", submitted to the Winter ANS Meeting, Washington D.C., 2004 (Sessions 10a and 10b, "US DOE NEER Highlights of Recent and Current Research I& II").